OPTICAL INVESTIGATION OF ION-METAL COLLISIONS

A Thesis

Presented to

The Faculty of the Graduate Division

by

William E. Baird, Jr.

In Partial Fulfillment

of the Requirements for the Degree

Doctor of Philosophy

in the School of Physics

Georgia Institute of Technology

November, 1975

OPTICAL INVESTIGATION OF ION-METAL COLLISIONS

Approved:

Edward W. Thomas, Chairman

Robert K. Preuss

James R. Stevenson

Date approved by Chairman: 13 Nov 1975

ACKNOWLEDGMENTS

I would like to thank my advisor, Dr. E. W. Thomas, for his guidance and encouragement throughout this undertaking. In addition to his skill as an experimental physicist, he also possesses untiring patience; these qualities make him an outstanding advisor. I would also like to thank Dr. Robert K. Feeney and Dr. James R. Stevenson for serving on my reading committee.

I would like to thank Dr. Maury Zivitz for his help during the early part of this research; Mr. James W. Larsen for his assistance with the computer calculations; and Mr. James E. Harriss for his assistance in the calibration procedure.

The expert typing of the final manuscript of this thesis is the work of Mrs. Lydia Geeslin and her daughter, Mrs. Lydia Sweatt.

Finally, for their encouragement and support during the years of my graduate program, I would like to thank my family.

TABLE OF CONTENTS

TABLE OF CONTENTS (Concluded)

LIST OF TABLES

LIST OF ILLUSTRATIONS

LIST OF ILLUSTRATIONS (Continued)

SUMMARY

Impact of 10 to 30 KeV H^+ or He^+ ions on polycrystalline metal surfaces causes some projectiles to be backscattered in a neutral, excited state. These projectiles subsequently radiatively decay, emitting Doppler-broadened spectral lines; the broadening is characteristic of the distribution in speeds and direction of the scattered excited projectiles. Analysis of the line shape shows that slow reflected particles have a high probability of losing the excited electron by a radiationless transition while they are close to the surface. The spectral line shape has been predicted using an established backscattering theory with the inclusion of a radiationless de-excitation term. By suitable choice of the radiationless de-excitation coefficient, the prediction may be fitted to the experimental data; thus the radiationless de-excitation coefficient may be determined.

In addition, quantitative measurements of total spectral intensity indicate that less than 1% of all projectiles are backscattered in an excited state. The relative variation of total spectral line intensity with angle of projectile incidence and with projectile primary energy has been predicted using a model which assumes that the probability for excited-state formation is independent of the energy and direction of the scattered projectile; the variation in total spectral line intensity with target atomic number is also predicted by this model. In each case, comparison is made with experimental measurements.

A brief study is made of sputtering and excitation of Al under He^+ impact; the measured intensities of observed spectral lines are presented as a function of He^+ incident energy.

Finally, negative results are obtained in a search for the existence of bound electron states in the wake of swift protons in aluminum and copper.

CHAPTER I

INTRODUCTION

Purpose of the Research

When 10-30 keV H^+ and He^+ ions are incident on polycrystalline metal surfaces, radiation in the visible and near-ultraviolet regions can be detected by optical methods. It is now well established that this radiation is emitted by three sources: (1) excited, neutralized, backscattered primary ions; (2) excited, sputtered target atoms or molecules; and (3) the solid itself. A major objective of this work has been the analysis of radiation emitted by the first source. Using information gained in this way, we have examined and predicted some of the physical interactions of the incident ions with the metal, ultimately determining the fraction of the incident ion flux which, after collision, is detectable through radiative decay. We have also made a limited investigation of photon emission from the second source and have searched for a proposed radiative phenomenon whose origin lies within proton-bombarded metal foils.

A description of the physical interactions of incident ions (particularly protons) with metal surfaces is of importance in understanding the behavior of a plasma within a thermonuclear reactor. Ions near the wall are lost mainly by charge exchange with the relatively large number of neutrals at the plasma surface; the neutralized ions then escape the magnetic field to impact on the wall. It is important to understand the ultimate fate of these impinging particles. Those which recoil in excited

states are relatively easily re-ionized and therefore re-populate the plasma. Thus the object of our research is of particular importance to an understanding of processes occurring within a thermonuclear reactor.

Our investigation of the photon emission of excited, neutralized, backscattered primary ions began as an extension and refinement of the work of Kerkdijk and Thomas.[1] They showed that when keV He^+ ions are incident on a metal surface, some of the projectiles are scattered as neutral, excited atoms. These atoms subsequently decay by photon emission. The resulting spectral line is Doppler-broadened, and the line shape is directly related to the distribution of speeds and distributions in angle of the scattered projectiles. Kerkdijk and Thomas developed a theoretical model for predicting these line shapes based on a number of simplifying assumptions. It was basically assumed that excited atoms were formed only from projectiles that were scattered by a single encounter with an atom in the surface of the target; this may be termed a "surface-scattering model." On this basis, the speed of a backscattered particle is dependent only on the angle through which it is scattered and the masses of the projectile and target atoms; hence the Doppler shift associated with a particular backscattered trajectory may be calculated. The angular distribution of the scattered atoms was assumed to be proportional to the Rutherford cross-section appropriate to the two isolated nuclei; hence relative probabilities of particular trajectories are known and the contribution to light intensity at the relevant Doppler shift may be evaluated. The line shapes calculated on this basis were in general qualitative agreement with the experimental data, but there were substantial quantitative discrepancies.

Our initial objective then was to test further the model of Kerkdijk and Thomas[1] with the hope of resolving the discrepancies between predicted and measured line shapes.

A serious fault in the surface-scattering theory is the neglect of projectile penetration into the target. McCracken and Freeman[2] have shown, both theoretically and experimentally, that most projectiles penetrate some distance before undergoing the large-angle scattering event which returns them to the surface. As the projectile proceeds to and returns from the scattering site, it suffers energy loss by collision with electrons (electronic stopping), but no appreciable deviation. As a result, the backscattered flux exhibits a distribution of energies with a peak flux at low energies. The work of Kerkdijk and Thomas[1] shows quite definitely that the backscattered excited-atom flux includes only small amounts of slow particles, so that one may conclude that slow excited atoms are de-excited while still close to the surface.

Two such de-excitation mechanisms have been discussed by Hagstrum[3] and by Varnerin.[4] In Figure 1 we illustrate the process known as resonance ionization. The excited atomic electron lies energetically above the conduction band of the metal and is therefore able, by tunneling, to occupy a state above the Fermi level. The condition on the energy parameters of the process is given by

$$E_i - E_x < \phi \tag{1}$$

where E_i and E_x are the ionization energy and the excitation energy, respectively, of the atom, and ϕ is the work function of the metal. Two

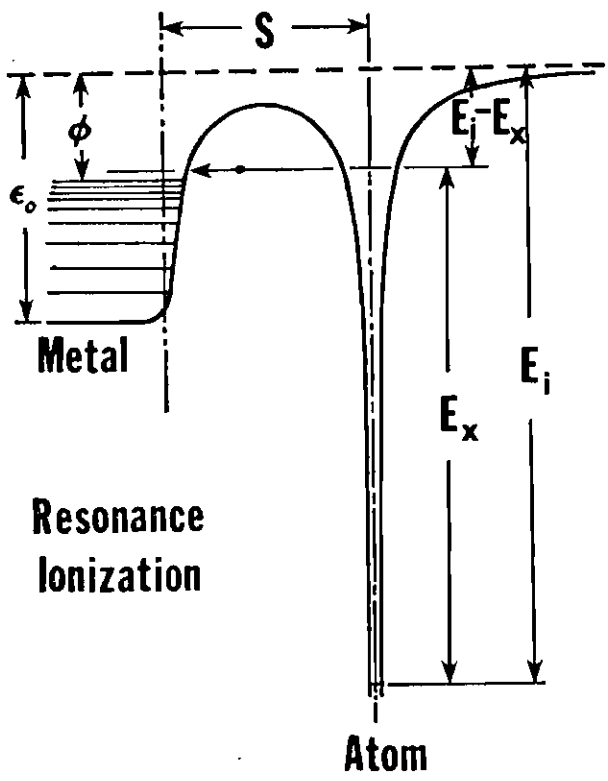

Figure 1. Resonance Ionization

further perturbations to the interaction are (1) the shift in atomic energy levels in the presence of the metal and (2) the image force between the ion and the metal surface. This process occurs for an atom-metal separation distance "s" of a few Ångstroms; e.g., for a metastable He(2^3S) atom at an Mo surface 2Å < s < 7Å. (The reverse process, resonance neutralization, occurs when an electron from an occupied state in the conduction band of the metal tunnels through the potential barrier to occupy an excited level of an ion near the metal surface, producing an excited, neutral atom. We make a brief reference to this later.) The other radiationless process, Auger de-excitation, is shown in Figure 2. Here a metal electron from within the conduction band falls into the ground state of the atom, releasing enough energy to eject the excited atomic electron to a continuum state. In this case the energy condition is given by

$$E_x > \phi \tag{2}$$

i.e., the excitation energy of the atom must exceed the energy required to remove an electron from the top of the conduction band. This interaction will not be perturbed by the image force, since the atom is electrically neutral both before and after the transition. The shift in atomic energy levels in the presence of the metal is, however, expected to be a perturbation, especially since this process occurs for a smaller atom-metal separation than that of resonance ionization; e.g., for a metastable He(2^3S) atom at an Mo surface s < 1Å.

Hagstrum has shown[3] that for small s the transition rate for either

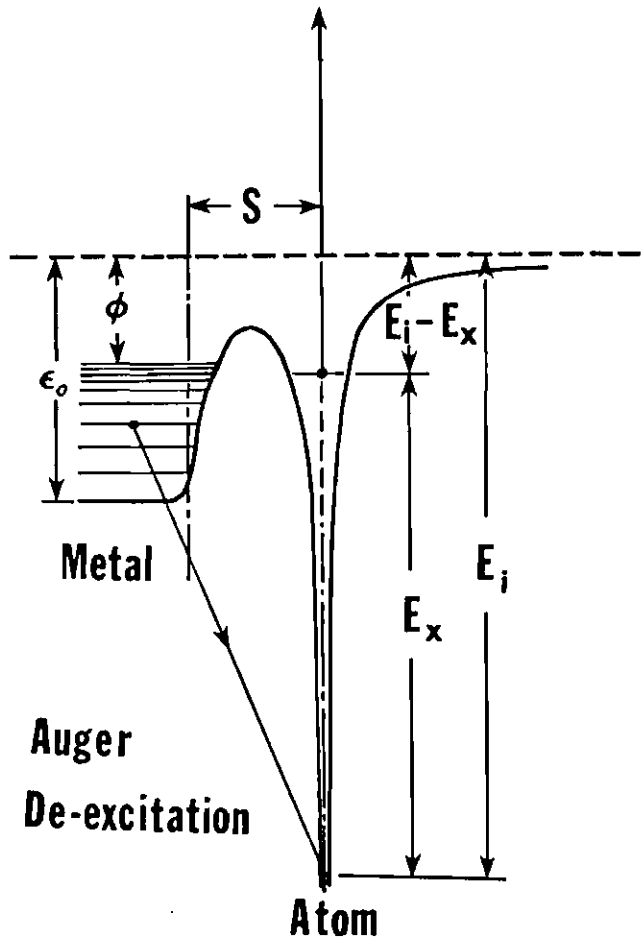

Figure 2. Auger De-excitation

mechanism can be approximated by

$$r(s) = A \exp(-as) \tag{3}$$

where A and a are constants related to the wavefunctions of the participating electrons and the form of the potential barrier. Thus, in this approximate form, we see that "A" is a measure of the maximum value of the transition rate, considering both kinds of transitions. Hagstrum also shows[3] that the parameter "a" is inversely proportional to the atom-metal separation for which the total probability of transition is a maximum. Furthermore, the probability that a receding particle having a velocity component $V_\perp$ normal to the surface of the metal will escape without radiationless de-excitation is[5]

$$p(V_\perp) = \exp(-A/aV_\perp) \tag{4}$$

Clearly the effect of these radiationless transitions is to remove the slow excited atoms. In fact, the ratio A/a may be thought of as a critical normal velocity component; backscattered atoms whose energies and directions are such that $V_\perp = A/a$ will have a probability of only 37% to escape without radiationless transition. Those whose normal velocity component is less than A/a will have a correspondingly lower probability of escape. We shall show that the Doppler-broadened line shape can be predicted by combining the scattered-particle velocity distribution of McCracken and Freeman[2] with the radiationless de-excitation factor described above; by suitable fitting of theory to experiment the ratio of parameters A/a in

Equation 4 may be derived. This ratio will henceforth be referred to as the "survival coefficient." Thus another objective of this work has been to determine the survival coefficient A/a for excited H and He atoms backscattered from a variety of metal surfaces (under H^+ and He^+ impact, respectively).

With these coefficients it is now possible to calculate how the total intensity of a line should vary with impact energy and with angle of incidence. One simply uses the derived coefficient A/a and integrates the predicted intensity distribution (line shape) over all wavelengths within the line; this is repeated for various angles of incidence and energies of impact. To provide an experimental quantity for comparison, we have measured the total intensity of a spectral line for various angles of incidence and energies of impact; to assign an absolute magnitude to these quantities, we have performed a calibration of our detection system. Using these absolute measurements of photon emission, we are thus able to establish the probability that an incident ion will be reflected as a neutral excited atom. We are further able to make some approximate conclusions regarding the probability of neutralization of an incident ion into a particular excited state.

In the case of backscattered, excited atoms, therefore, we have investigated both theoretically and experimentally the dependence of photon emission on angle of incidence and on impact energy for a given incident-ion/target-atom combination. We have studied one other functional dependence for photon emission from this source. For a given incident ion species, impact energy, angle of incidence, and spectral line, we have

measured photon emission as a function of target material. Our prediction for this dependence comes from the work of McCracken and Freeman[2]: a factor involving the atomic numbers of the incident and target species (which is omitted in our relative prediction of line shape) has been used as our model.

We have detected photon emission from excited, sputtered target atoms in the case of He^+ incidence on Al (the heavier projectile species and the lightest target species) and have measured the photon emission for two of the observable spectral lines as a function of impact energy. We do not present a theoretical model for this dependence, but do determine the rate of formation per incident ion for the excited state involved

Finally we shall present the results of our search for the existence of bound electron states in the wake of swift protons in Al and Cu, as proposed theoretically by Neelavathi, Ritchie, and Brandt.[6]

Review of the Literature

Among the first to observe photon emission during ion impact on metals were Chaudhri et al.,[7] who used 200-2500 eV He^+ ions on a sheet of Ni; they detected radiation characteristic of the decay of excited He atoms. Sterk et al.[8] made quantitative measurements of Lyman alpha emission induced by keV protons incident on Al; they found that the number of Lyman alpha photons emitted per incident proton was of the order of 10^{-3}. Gritsyna et al.[9] studied the emission induced by 20 keV H^+ and H_2^+ impact on surfaces of Cu and Ta; they observed the first three lines of the Balmer series of hydrogen; broadening of these lines was ascribed to Doppler shifts of emission from the scattered projectiles. In addition, Gritsyna

et al.[10,11] detected atomic and molecular He emissions induced by 20 keV He^+ ions on metal surfaces; they, however, determined[11] that the emissions were principally due to the interaction of the primary beam with a carbon film deposited on the metal surfaces; thus the observations tell us nothing about the interaction of He^+ with a pure metal surface. There is also a study by McCracken and Erents[12] of the Lyman alpha line induced by keV proton impact on Mo; shifts of emission to shorter wavelengths and to longer wavelengths are ascribed to Doppler shifts on direct and reflected photons, respectively. One of the most recent studies of radiation emitted by backscattered particles has been the work of Kerkdijk and Thomas.[1] For the case of 2-10 keV proton impact on Cu, they observe the first three lines of the Balmer series; for 2-10 keV He^+ impact on Cu, they observe the following lines of HeI: 3889 Å($3^3P \rightarrow 2^3S$), 5876 Å($3^3D \rightarrow 2^3P$), 4472 Å ($4^3D \rightarrow 2^3P$), and 4026 Å($5^3D \rightarrow 2^3P$). They also found that use of neutralized ions for the incident species produced essentially the same spectral characteristics in both cases. We have already mentioned their prediction of line shape (for He lines); they also predict the emission intensity per incident ion for three of the observed He lines as a function of angle of incidence, with comparison to experimental findings. Experimental measurements are also presented of emission intensity per incident ion for each of the observed He and H lines as a function of impact energy; no attempt is made to predict this dependence theoretically.

Sputtering and excitation of Cu atoms by 80 keV Ar^+ impact on a Cu surface have been studied by van der Weg and Bierman,[5] who found evidence of radiationless transition of the excited Cu atoms. They derived the probability given in our Equation 4 from the transition rate in our

Equation 3, and determined a value of A/a of 2×10^6 cm /sec by fitting their theory to an observed Cu line shape. For lower-energy projectiles (10-3000 eV Ar^+) on a Cu surface, White and Tolk[13] also observed radiation characteristic of excited, sputtered Cu atoms. The emission per incident ion was analyzed as a function of impact energy, and this dependence was predicted by assuming the possibility of radiationless de-excitation. A fitting of the prediction to the experimental data yielded a value of A/a of 2×10^6 cm /sec , in agreement with van der Weg and Bierman.[5] Tolk et al.[14] suggested that backscattered particles are also subject to radiationless transition as they recede from a metal surface; the probability of such a transition was seen to be dependent on the band structure of the solid, being much more likely for metals than for insulators; they also observed broad band continuum radiation arising from the bombarded metal itself. Broad band radiation has also been observed by Kerkdijk and Thomas[1] in the region 3000-4000 Å for H^+ and He^+ incidence on Cu; they have examined the intensity of this phenomenon as a function of projectile incidence angle and as a function of projectile impact energy. A recent explanation of broad band phenomena in H^+ and He^+ bombarded Al, Cu, and Mo, which employs an electron-hole recombination model, has been given by Zivitz and Thomas.[15]

Concerning the energy distribution of the backscattered particles, we have already mentioned the work of McCracken and Freeman.[2] They presented theoretical (single-collision) and experimental determinations of the energy distributions of protons and deuterons backscattered from Ti and Nb. Very good agreement was obtained for Ti, while slightly inferior agreement in the case of Nb suggested the possibility of multiple

scattering. Their energy distribution is somewhat supported by the work of Meischner and Verbeek,[16] who found that the flux of backscattered hydrogen atoms and ions is a decreasing function of their recoil energy, with a high-energy cut-off at the primary impact energy. Unlike McCracken and Freeman, they show a pronounced maximum in the distribution around 1 keV with a sharp drop-off for lower energies. An entirely different energy distribution for backscattered ions (experimental) and ions-plus-atoms (theoretical) has been presented by Firsov et al.,[17] who show a maximum backscattered flux near the primary impact energy for 30 keV He^+ impact on Cu, Al, and Ge; their model assumes multiple scattering of the incident projectiles by the target atoms. Erickson and Smith[18] have shown that the backscattered He^+ ion yield has an oscillatory dependence on primary ion energy, for 200-2000 eV He^+ impact on Pb, Ge, and Bi; the explanation for this behavior lies in repeated resonant electron transitions between the ions and the solid.

The theoretical determinations of survival coefficient A/a are primarily found in the publication of Hagstrum,[3] who interprets the work of Shekhter[19] and of Cobas and Lamb.[20] Shekhter is concerned with the neutralization of positive ions at a metal surface and performs a calculation of resonance neutralization for protons at an Mo surface. Hagstrum interprets this to get a value of $A/a = 1.8 \times 10^{11}$ cm /sec for resonance processes in general (both neutralization and ionization). Cobas and Lamb perform calculations for both resonance neutralization of He^+ at an Mo surface and Auger de-excitation of $He(2^3S)$ at an Mo surface, employing hydrogenic wavefunctions for the He^+ ion and He atom. According to Hagstrum, this yields $A/a = 4.8 \times 10^{10}$ cm /sec for resonance processes and

$A/a = 1.3 \times 10^8$ cm /sec for Auger de-excitation. Using a somewhat different approach, Gersten and Tzoar[21] have suggested that when the energy of an allowed atomic transition is slightly greater than the surface plasmon energy of a metal, de-excitation of an atom at the metal surface may result in a surface plasmon emission, rather than the creation of a photon. For the case of a Lyman beta transition in an H atom at an Al surface, they calculate for this process an A/a of 6.12×10^7 cm /sec Since this type of de-excitation may be in competition with the previously discussed radiationless processes, the value of A/a determined by experiment may differ considerably from this depending on the relative strengths of the various de-excitation processes. For the case of heavier incident projectiles, Janev et al.[22] performed calculations for Li^+, Li, and Na^+ impact on Mo and W; for resonance processes they derive values of A/a from 3.2×10^{11} cm /sec to 1.5×10^{13} cm /sec.

Of all the literature, perhaps the most immediately relevant to the present work is the material presented in the doctoral dissertations of Smits[23] and Kerkdijk.[24] They predict the shape of the Doppler-broadened Balmer beta line emitted by backscattered, excited H atoms, but nowhere made a direct comparison with experiment. They do make a comparison between theory and experiment for the dependence of this spectral line on impact energy and angle of incidence; however the quantities which are compared are the positions of the maximum intensity and the relative magnitudes of the maximum intensity. It would seem that the integrated intensity which we use would be less subject to statistical error. By fitting these theoretical quantities to their data they also determine a value for the survival coefficient, $A/a = 1.5 \times 10^8$ cm /sec , for 10-40

keV protons incident on Cu. One simplifying approximation which they make is the neglect of photons reflected by the target to the observer. This reflected light we have found to be of considerable importance in obtaining agreement between our theoretical line shape prediction and the observed form of the spectral lines.

CHAPTER II

EXPERIMENTAL ARRANGEMENT

Preface

Most of the experimental work was done using H^+ and He^+ ions of 10-30 keV energies; the apparatus used for this work will be described at length in the following sub-headings. In addition, a small amount of time was spent using a Van de Graaf accelerator and its supporting equipment; this will be treated briefly in the final sub-heading.

Introduction

The experimental arrangement for the 10-30 keV apparatus is shown schematically in Figure 3. The H^+ or He^+ ions obtained from an rf discharge source were mass-analyzed, collimated, and directed onto the target surface at some incidence angle $\emptyset$ with respect to the target surface normal. A grating monochromator viewed the surface through a sapphire window; the monochromator axis was perpendicular to the projectile beam direction and lay in the same plane as the projectile beam and the target surface normal. The monochromator was fitted with a photomultiplier detector operated in the counting mode; the spectral line shape was recorded by scanning the monochromator.

Ion Source and Accelerator

Ionized hydrogen or helium was supplied by an Ortec Model 320 radio-frequency ion source consisting of a Pyrex bottle with gas inlet, aluminum

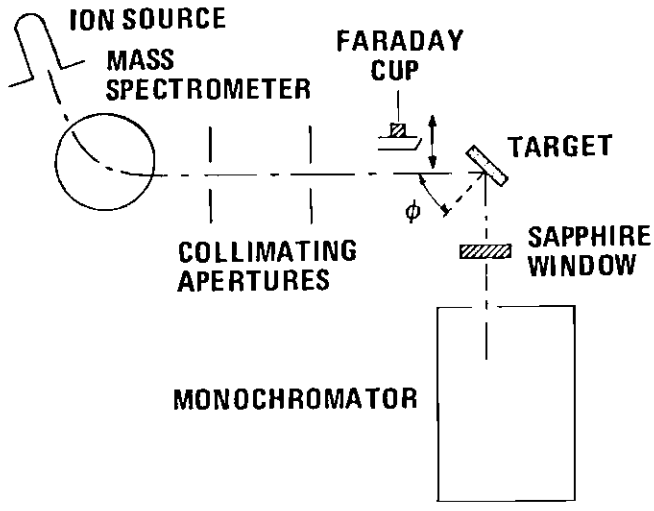

Figure 3. Schematic Diagram of the Apparatus

tip, and sapphire sleeve, a radio-frequency oscillator, and a magnet providing an axial field. An extraction voltage of 0-5 keV across the bottle provided the initial acceleration, while additional acceleration to provide total energies of 10-30 keV was supplied by a Sorensen 5030-4 power supply. The source and its power supplies were maintained at high potentials, requiring insulation from the rest of the apparatus. Also the source was shielded to prevent radio-frequency pick-up in the recording electronics.

Immediately upon leaving the source bottle, the ions were focused by an Einzel lens. Separation of H^+ ions from other ions (H_2^+ and H_3^+) was made by magnetic deflection; likewise He^+ ions were isolated from gaseous impurities. Current to the magnet was supplied by a Hewlett-Packard 6296A regulated current supply. The H^+ or He^+ beam was deflected 30^o from its initial direction into a beam pipe of approximately 2 meters length, which contained a second Einzel lens and two pairs of deflection plates.

The source region was pumped by a Consolidated Electrodynamics Corporation oil vapor diffusion pump and maintained at a pressure of approximately 10^{-6} Torr. The beam pipe was pumped by two cold-trapped Edwards oil vapor diffusion pumps (Model E02) and maintained at a pressure of approximately 10^{-7} Torr.

Target Chamber and Sample Holder

The ion beam traveled from the beam pipe into the target chamber, which was maintained at a base pressure of 10^{-9} Torr by an Ultek Model 10-402 Boostivac ion pump. The targets were mounted on a standard Varian manipulator (Model 981-0523) which permitted rotation of the target to

obtain the desired angle of incidence $\emptyset$ between the beam direction and surface normal. The manipulator also allowed both vertical and horizontal translation of the target which permitted alignment of the system, with the axis of rotation intersecting the optical and projectile beam axes.

Optics and Electronics

The emitted photons were transmitted by the Varian UV grade single-crystal sapphire window and received by the monochromator, a Jarrel-Ash Model 84-110. The monochromator was fitted with a photomultiplier detector (EMI 9558) operated in the counting mode. (For examination of spectra in the region below 3000 Å, a photomultiplier EMI 6256 was temporarily inserted.) The optical signal was transmitted by the electronics (see Figure 4) and recorded by a Teletype or a pen-recorder. Also the beam current was monitored on a Faraday cup, which could be inserted to the beam line periodically; this signal was monitored on an electrometer (Keithley Model 415), converted to a digital signal by a voltage-to-frequency converter, then scaled and periodically recorded on the Teletype.

Operating Procedure

The targets were polycrystalline metals of high purity (99.97%). Before use, the samples were mechanically polished or electropolished, and cleaned with solvents (see Appendix). For the case of polycrystalline Mo under proton impact, we found that the method of polishing used made negligible difference in the observed line shape. The samples were mounted in the target chamber on a standard Varian manipulator. By adjusting the position of the target holder as described above, it was possible to fix accurately the position of the beam on a particular target;

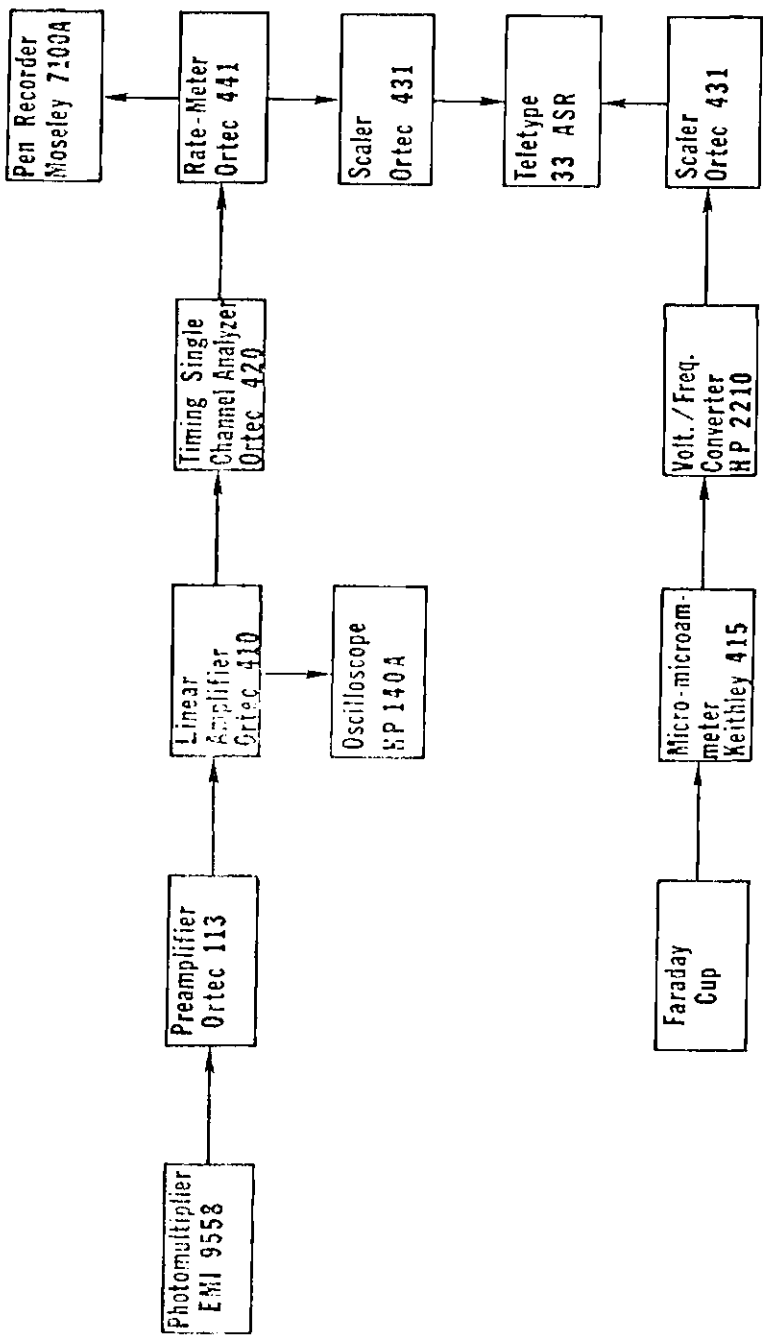

Figure 4. Data-Collecting Electronics

the position was first approximately located by visual inspection, then the beam current was maximized on that particular target to achieve exact positioning of the target.

Projectile beam currents were monitored on a Faraday cup that could be inserted to the beam line periodically. The current measured on the target itself was used to monitor beam stability during optical measurements; this target current was not considered to be a reliable measure of the projectile flux because it was impossible to guarantee complete suppression of all secondary ejected particles. Currents were typically 1-10 μA in a beam of about 1 $mm.^2$ cross-sectional area.

The projectile beam flux was sufficient to sputter off a few monolayers of target material every minute. It is felt that a preliminary bombardment of the surface with the ion beam itself is sufficient to guarantee target cleanliness. It was found that the optical signals showed some variation with time for a few minutes after the beam was directed at a new target; beyond that point the signals remained stable for many hours. Data taken during the first few minutes of bombardment were discarded. In certain instances the target surfaces were initially bombarded with Ar^+ ions to clean them further by sputtering; the signals observed thereafter under H^+ or He^+ bombardment showed no significant difference from the case of un-sputtered targets.

Complete spectra (3000-7000 Å) for various ion-metal combinations were recorded by a pen-recorder; the beam current, as measured on the Faraday cup, was recorded both before and after each spectrum with the stability of the beam current during the run monitored on the target.

When a single emission line was studied, the Ortec scalers were used in a two-phase cycle. For the first phase, the beam current was incident on the Faraday cup; the current was monitored on an electrometer and digitized for recording on a scaler. This was continued for a certain time interval (40-80 sec.) and the count was then printed out by the Teletype; also during this phase the background signal of the photomultiplier was measured and printed out. During the second phase (of equal duration), the Faraday cup was removed so that the beam could strike the target; the emitted photons were detected by the photomultiplier and counted on a scaler; finally, after the preset time interval, the count was printed out. Thus a ratio of emission to incident ion flux could be determined. Several (four to eight) such cycles were completed at each wavelength of interest, and the ratios were averaged to reduce statistical error.

Calibration

In order to determine the intensities of the spectral lines in photons per incident ion, it was necessary to calibrate the detection system. A lamp (EPS-1047) calibrated by the Eppley Laboratories according to the method of the National Bureau of Standards[25] was used as the primary standard for the visible spectrum. A Phillips tungsten-filament lamp (E-256) was used as the secondary standard because of its more convenient size. In order to extend the calibration to include ultraviolet wavelengths (3000-4000 Å), the branching ratio method was employed.[26,27] Nitrogen gas was introduced into the target chamber and excited by a 25 keV beam of H^+ or He^+ ions. Observations were made of the relative signals from the second positive system of N_2 and the first negative system of N_2^+.

Theoretical predictions of the relative intensities in these two spectral systems were obtained from the work of Thomas et al.[28] and Burns et al.[29] Hence the relative sensitivity was established and could be normalized to the absolute sensitivity measured at visible wavelengths using the standard lamp.

Apparatus for 1.0 MeV Range

This experimental arrangement is quite similar to that discussed above. The H^+ ions obtained from a Van de Graaf accelerator were mass analyzed, collimated, and directed onto the target at some incidence angle $\emptyset$ with respect to the target-surface normal. A grating monochromator viewed the surfaces (front and back) through a quartz window; the monochromator axis was perpendicular to the projectile beam direction and lay in the same plane as the projectile beam and the target surface normal. The monochromator was fitted with a photomultiplier detector operated in the counting mode; the ultraviolet and visible spectrum was recorded by scanning the monochromator.

The targets were thin foils ($\lesssim 1\ \mu$) of Al and Cu. The Al foils were supplied by A. D. Mackay, Inc.; the Cu foils were made by a thin-film deposition process in the Engineering Experiment Station. The samples (enclosed and supported by thin plates of Cu) were mounted in the vacuum system on a standard Varian manipulator. It was possible to rotate the sample to change the angle of beam incidence $\emptyset$, and also translate the sample to insure that the axis of rotation intersected the optical and projectile beam axes. By proper choice of the angle of incidence, the target could be oriented so that the monochromator viewed either the

frontside of the target or the backside of the target. The vacuum environment of the target was maintained by cold-trapped oil diffusion pumps at a base pressure of 10^{-6} Torr.

Projectile beam currents were monitored on a Faraday cup which was located beyond the target; thus the target had to be raised vertically out of the path of the beam in order to measure the beam flux. During bombardment of the foils, the stability of the beam was monitored by observing the transmitted, undeflected fraction which was incident on the Faraday cup. Total currents were typically 10^{-7} to 10^{-6} amperes, and the amount of transmitted, undeflected beam was one to two orders of magnitude lower. The electronics for transmission and recording of the data were identical to those illustrated in Figure 4, except that a pen-recorder was used exclusively for the recording of data (i.e., the scalers and Teletype were not used).

CHAPTER III

EXPERIMENTAL OBSERVATIONS

General Spectral Characteristics

For each ion-metal combination used, we first ran a complete recording of the spectrum to determine what types of emission were present. For 20-30 keV He^+ incident on Cu, Nb, Mo, Ag, and W, there were emissions of the following He I lines: 5876 Å ($3^3D \rightarrow 2^3P$), 4472 Å ($4^3D \rightarrow 2^3P$), 3889 Å ($3^3P \rightarrow 2^3S$), and 6678 Å ($3^1D \rightarrow 2^1P$). In the case of He^+ on W, there were also He I emissions at 4026 Å ($5^3D \rightarrow 2^3P$), 4713 Å ($4^3S \rightarrow 2^3P$), and 4922 Å ($4^1D \rightarrow 2^1P$); the intensities of these latter emissions were smaller by a factor of four than the former. Also apparent in these spectra were various broad band phenomena whose origin we did not pursue. In Figure 5 we show a sample strip-chart recording of the spectrum observed for the case of He^+ ions incident on Cu. The wavelength labeling is according to the monochromator scale, whose offset varies from + 16.6 Å at the low wavelength end to + 17.5 Å at the high wavelength end. The principal broad band in this case is centered about 3250 Å.

For 20-30 keV H^+ on these metals, there were emissions of the following H lines: H_α 6563 Å (n = 3 to n = 2), H_β 4861 Å (n = 4 to n = 2), and H_γ 4340 Å (n = 5 to n = 2). As in the case of He^+ incidence, we observed various broad band emissions. (These broad band emissions are described briefly in the paper[15] by Zivitz and Thomas.) In Figure 5, we also show a sample strip-chart recording of the spectrum observed for the

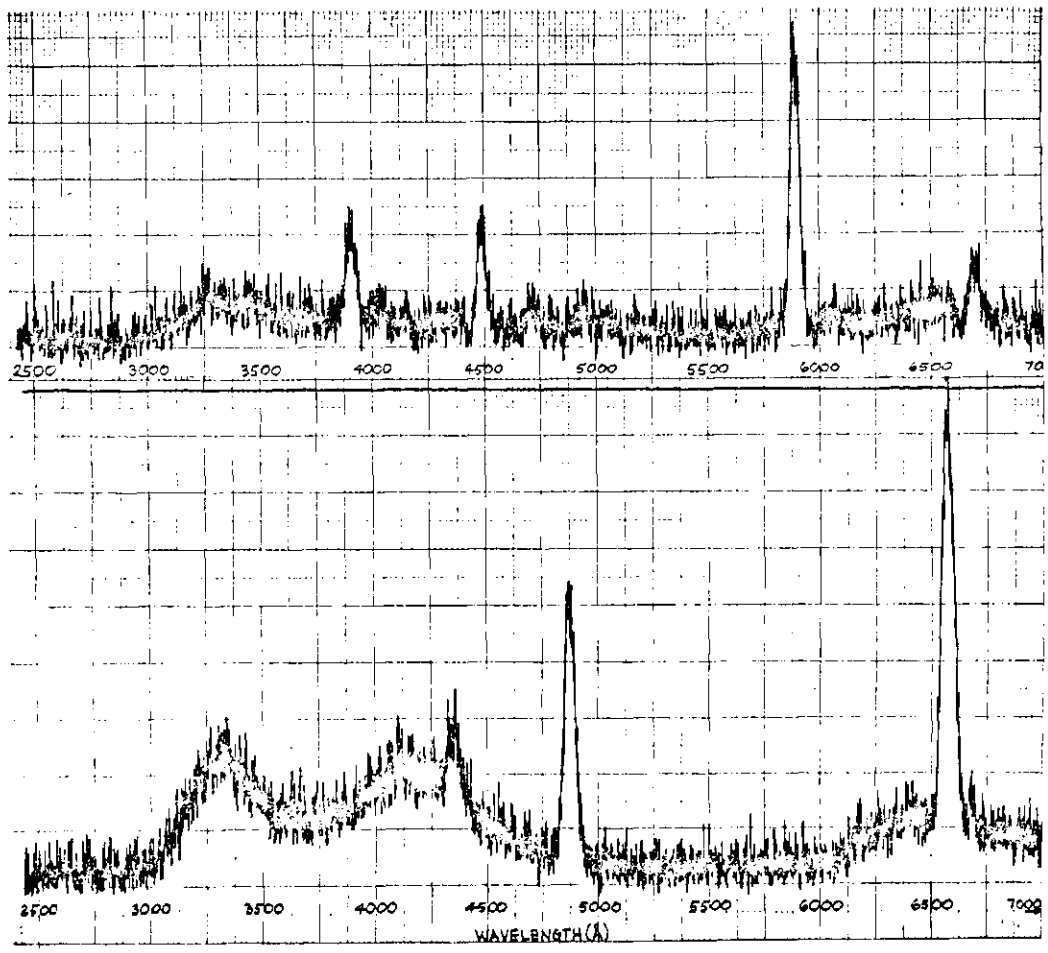

Figure 5. Strip-Chart Recordings of the Observed Spectra. (Upper: 25 KeV He^+ incident on Cu at an angle of 60^o. Lower: 25 KeV H^+ incident on Cu at an angle of 60^o.)

case of protons incident on Cu. The principal broad bands in this case are centered about 3250 Å and 4200 Å.

For both He^+ and H^+ incidence on Al we observed a very intense broad band extending from 2500 Å to 6000 Å with a maximum at 5200 Å which obliterates the usual lines from scattered projectiles except for He 5876 Å and H_α 6563 Å, respectively. (This broad band is dealt with in detail in the paper[15] by Zivitz and Thomas.) For the case of the Al target bombarded by He^+, we observe emissions of Al I lines including all components of the multiplets at 3089 Å and 3956 Å. For these lines we observe no broadening or wavelength shifts that can be attributed to the Doppler effect. It is therefore concluded that the sputtered, excited Al atoms are ejected with rather low velocities. Tests were made to ascertain whether any of the emissions exhibit polarization; this was performed simply by monitoring the light signal as a polaroid analyzer was rotated in front of the monochromator. No evidence of polarization was found.

Broadening of Spectral Lines

Detailed study of the He I lines and H lines indicates that they are of the order of 50 Å and 100 Å in breadth, respectively, with a sharp peak on the blue side. In Figure 6 we show a number of measurements on the 5876 Å ($3^3D \rightarrow 2^3P$) line. It is observed that, as incidence angle increases, the line width broadens and total intensity increases. There is an obvious sharp peak on the low-wavelength (blue-shifted) side of the line. The broadening of the spectral lines may easily be shown to be a consequence of the Doppler effect on emissions from the fast scattered atoms. Consider the case of an excited, backscattered 30 keV He atom

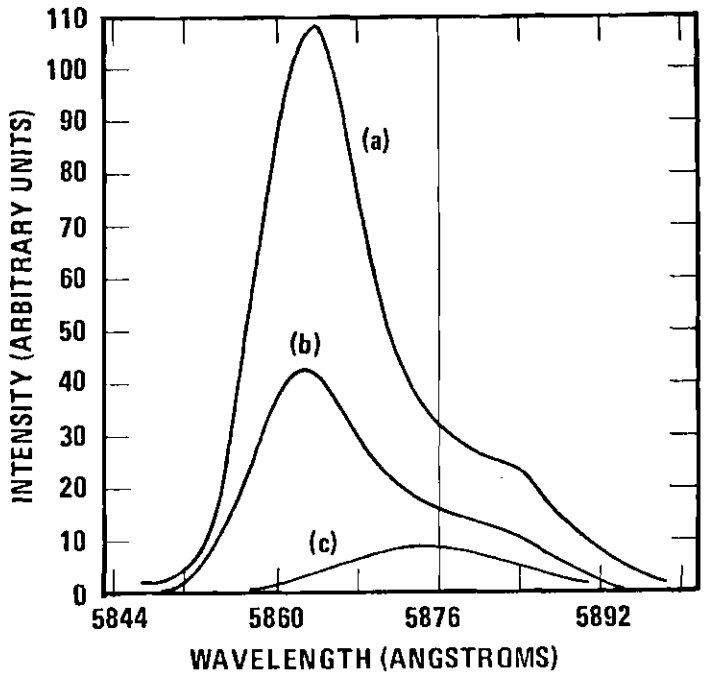

Figure 6. Experimental Line Shapes of the 5876 Å ($3^3D \rightarrow 2^3P$) He I Emission. (Experimental conditions: 30 KeV He^+ incident on Nb at an incidence angle $\emptyset$ of (a) 60°, (b) 45°, and (c) 0°. Only a smoothed curve is shown.)

which emits a 5876 Å photon as it decays from the state 3^3D to the state 2^3P. If the trajectory of the atom is toward the observer (monochromator), the non-relativistic Doppler formula predicts a shift of - 24 Å from the nominal wavelength (5876 Å); if the trajectory is along the surface of the target away from the observer (and assuming an incidence angle of 60^o), the shift predicted is + 12 Å. In addition, the atom may emit a photon 180^o away from the observer which is then reflected by the metal surface; because this trajectory is opposite to the path which produces a blue shift, a contribution to the red-shifted side of the line is provided by these reflected photons. In Figure 6, curve (a), we see that essentially all of the Doppler-broadened 5876 Å line is included between the calculated shifts of - 24 Å and + 12 Å. For the case of an excited, backscattered 30 keV H atom which emits a 6563 Å (Balmer alpha) photon as it decays from the state n = 3 to the state n = 2, the Doppler shifts associated with the two trajectories described above are - 52 Å and + 26 Å, respectively. For a given recoil energy, an H atom will have twice the velocity of an He atom; thus the Doppler shift of the photon emission from an H atom will be approximately twice that for an He atomic emission, for the two transitions considered here. It should also be expected that as the initial projectile energy decreases, the spectral line width decreases, contracting about the unshifted nominal wavelength for the transition. It will be recalled that McCracken and Erents[12] explained the broadening of Lyman alpha radiation induced by keV photon impact on Mo as due to Doppler shifts on the direct and reflected photon emission.

Thus in principle the Doppler-broadened line shape contains information on the distributions in energy and angle of the scattered projectiles.

In Chapter IV we will discuss how the line shape can be analyzed to provide this information and will present sample He and H line shapes, both experimental and predicted.

Total Intensity of the Line Emission

A major objective of this work was to establish an absolute measurement of the total light intensity emitted in a transition; clearly this can be related to the probability that an incident ion will recoil in a specific excited state. A convenient representation, suggested by Kerkdijk and Thomas,[1] is to define a coefficient γ_{jk} for emission of photons in a transition from state j to state k; this coefficient is simply the total number of photons emitted into all directions per incident projectile. A second valuable factor[1] is the coefficient γ_j for formation of a specific excited state j; this can be defined as the number of backscattered atoms in the state j per incident projectile. In a special case where an excited state j cannot be populated by cascade from higher levels i and where the transition $j \rightarrow k$ is the only decay path, then γ_j will equal γ_{jk}. In general this is not true; the state j is populated by cascade from higher levels i and is depopulated by more than one radiative decay path; consequently γ_j and γ_{jk} are not equal. The general relationship between the emission and excitation coefficients is given by[1]

$$\gamma_{jk} = \left\{ \gamma_j + \sum_{i>j} \gamma_{ij} \right\} \times \frac{A_{jk}}{\sum_{k<j} A_{jk}} \qquad (5)$$

where only allowed transitions are considered and A_{jk} represents the

transition probability for the transition $j \rightarrow k$ as tabulated.[30] In words, the emission coefficient for the transition $j \rightarrow k$ equals the product of (1) the sum of the excitation coefficient to the state j and the cascade into j from all higher states i and (2) the ratio of the transition probability for $j \rightarrow k$ to the sum of all probabilities for transition out of j. This may be rewritten as

$$\gamma_j = \frac{\sum_{k<j} A_{jk}}{A_{jk}} \gamma_{jk} - \sum_{i>j} \gamma_{ij} \qquad (6)$$

or, equivalently,

$$\gamma_j = \sum_{k<j} \gamma_{jk} - \sum_{i>j} \gamma_{ij} \qquad (7)$$

These relationships between excitation and emission coefficients are analogous to the relationship between excitation and emission cross sections in atomic collisions studies.[31]

The emission coefficient, γ_{jk}, has been measured in this experiment. The line shape of a transition is scanned and integrated; the calibrated sensitivity of the detection system permits this to be converted to an absolute photon flux. We make the assumption that the emission is isotropic. It is known that photon emission from decay of np and nd states may exhibit polarization if populations of the different magnetic quantum number substates are not equal. Furthermore, if emission is polarized, then it will exhibit an anisotropic spatial distribution. Such anisotropies are well known in studies of excited state formation as projectiles traverse gas targets under single-collision conditions; the projectile is

essentially undeviated by the collision and the direction of projectile motion defines a quantization axis. We must inquire whether a similar situation might occur for atomic scattering from a solid. We would first note that the average recoil velocity of an excited atom is of the order 10^8 cm /sec and its lifetime is of the order 10^{-8} sec ; the distance at which radiative decay occurs is some millimeters from the surface; this is far enough from the target to preclude any interaction between the photon emission and the metal surface. Thus any anisotropy or polarization must be related to the process of excited atom formation and not to the radiative decay. Since projectiles are scattered into 2π steradians, there is no obvious direction of quantization associated with the problem. Moreover, if there were some preferential axis for quantization, then one would expect the emission to be polarized; no polarization is observed. We therefore feel that the assumption of isotropic emission is justified. Thus under this assumption we arrive at the total emission rate by multiplying the photon flux into the monochromator by $4\pi/\Delta\omega$; here $\Delta\omega$ is the solid angle subtended at the target by the monochromator entrance slit. Taking this photon emission rate and dividing by projectile ion flux we obtain a value for γ_{jk}.

For a given transition, a ratio between emission coefficients determined for various angles and energies of impact is reliable within $\pm$ 10%; the principal source of possible error is the statistical variation of signals. In comparing emission coefficients for two different transitions there is an additional source of possible error in the relative calibration of detection sensitivity at different wavelengths. The factors which influence the reliability of the relative calibration are (1) the

determination of the intensity of the secondary standard at various wavelengths, whose percent uncertainty is ± 15%; (2) the transmission-versus-wavelength of the neutral density filter (used to limit the light intensity incident on the monochromator), whose percent uncertainty is ± 6%; and (3) the statistical variation of the signals recorded in the calibration, ± 6%. Finally, in addition to these factors, the absolute calibration is affected by the reproducibility of various geometrical parameters, ± 8%. (The operating conditions for which the primary standard lamp was calibrated were established by setting the lamp current rather than temperature; with the lamp operating at the specified current, the manufacturers assigned a reliability of ± 1/4% to the values of spectral radiance-versus-wavelength supplied with the lamp.) Thus the uncertainty in a particular absolute emission coefficient is the sum of the above uncertainties, plus a ± 3% uncertainty in the calibration of the electrometer, or 48%.

In Tables 1 through 3 we display some of these measured emission coefficients for the case of backscattered particles. They may be shown as a function of incidence angle on a particular target for a fixed projectile energy (Table 1); as a function of impact energy for a fixed incidence angle and specific ion-target combination (Table 2); or as a function of the target atomic number for a fixed projectile energy and incidence angle (Table 3).

For comparison purposes we show in Table 4 the emission coefficients for certain transitions induced by 25 keV H^+ and He^+ on Mo at an angle of 60 degrees to the surface normal. In a few cases we have estimated the excitation coefficient γ_j. The excitation coefficient for the 3^3P state was estimated by allowing for cascade from higher n^3S and n^3D levels

Table 1. Emission Coefficient of the Hydrogen n = 3 to n = 2 Transition Shown as a Function of Angle of Incidence for 25 KeV Protons Incident on Niobium

Angle of Incidence (degrees)	Emission Coefficient γ_{jk} (photons/proton)
0	4.62×10^{-5}
15	4.78×10^{-5}
30	6.85×10^{-5}
45	9.80×10^{-5}
60	13.9×10^{-5}

Table 2. Emission Coefficients for Backscattered Particles as a Function of Impact Energy

Experimental Conditions	Transition	Emission Coefficient γ_{jk} (photons/ion) vs. impact energy				
		10 KeV	15 KeV	20 KeV	25 KeV	30 KeV
H^+ on Mo at 45° incidence	H_α (n = 3 to n = 2)	1.14×10^{-4}	1.04×10^{-4}	0.872×10^{-4}	0.741×10^{-4}	0.647×10^{-4}
H^+ on Cu at 45° incidence	H_α (n = 3 to n = 2)	0.762×10^{-4}	0.686×10^{-4}	0.585×10^{-4}	0.519×10^{-4}	0.486×10^{-4}
He^+ on Mo at 45° incidence	He I $3^3P \rightarrow 2^3S$	4.06×10^{-6}	4.74×10^{-6}	4.94×10^{-6}	5.05×10^{-6}	5.65×10^{-6}
He^+ on Cu at 45° incidence	He I $3^3P \rightarrow 2^3S$	3.20×10^{-6}	3.29×10^{-6}	3.69×10^{-6}	3.74×10^{-6}	4.09×10^{-6}
He^+ on Cu at 45° incidence	He I $3^3D \rightarrow 2^3P$	0.933×10^{-5}	1.43×10^{-5}	1.83×10^{-5}	2.37×10^{-5}	2.34×10^{-5}

Table 3. Emission Coefficients for Backscattered Particles as a Function of Target Atomic Number

Experimental Conditions	Transition	Emission Coefficient γ_{jk} (photons/ion) vs. target atomic number					
		Al Z = 13	Cu Z = 29	Nb Z = 41	Mo Z = 42	Ag Z = 47	W Z = 74
25 KeV H^+ ions incident at 60°	H_α n = 3 to n = 2 (6563 Å)	0.820×10^{-4}	1.39×10^{-4}	1.39×10^{-4}	1.62×10^{-4}	3.64×10^{-4}	3.29×10^{-4}
25 KeV He^+ ions incident at 60°	He I $3^3D \rightarrow 2^3P$ (5876 Å)	2.94×10^{-5}	4.52×10^{-5}	5.68×10^{-5}	8.34×10^{-5}	11.6×10^{-5}	17.5×10^{-5}

Table 4. Measured Emission Coefficients and Estimated Excitation Coefficients. (Data for H^+ and He^+ ions at 25 keV incident on a Mo target at angle of 60° to the surface normal.)

Projectile	States		γ_{ij}	γ_i
	i	j	(Photons/ion)	(Excited atoms/ion)
H^+	n = 3	n = 2	1.62×10^{-4}	
H^+	n = 4	n = 2	1.89×10^{-5}	
H^+	n = 5	n = 2	4.92×10^{-6}	
He^+	3^3D	2^3P	8.34×10^{-5}	8.17×10^{-5}
He^+	4^3D	2^3P	9.04×10^{-6}	1.15×10^{-5}
He^+	3^3P	2^3S	9.38×10^{-6}	6.10×10^{-6}

(about 42%) and branching of the decay between $3^3P \rightarrow 2^3S$ and $3^3P \rightarrow 3^3S$ transitions; transition probabilities were obtained from the work of Wiese et al.[30] For estimates of γ_j for the 4^3D state, we had no way of assessing cascade and, for the 3^3D, could estimate cascade only from the 4^3P level (about 2%); consequently the values of γ_j are not really corrected for cascade and include only corrections for branching in the decay transition. For the hydrogen emissions we did not attempt to estimate γ_j; the measured Balmer emission is a sum of three transitions from the almost-degenerate ns, np, nd states to the lower 2s and 2p levels; there is no way of estimating the relative importance of the separate transitions.

Concerning the He states 4^3D and 3^3D for which we could not make accurate determinations of total cascade, we have made some estimates based on certain assumptions. By assuming the He (n = 5) states to be roughly equally populated, we estimate that approximately 10% of the quoted value for $\gamma_4{}^3{}_D$ (in Table 4) is due to cascade from 5^3P and 5^3F. Under this same assumption we estimate that approximately 2% of the quoted value for $\gamma_3{}^3{}_D$ is due to cascade from 5^3P and 5^3F; by assuming that the He (n = 4) levels are roughly equally populated, we estimate that approximately 18% of the quoted value for $\gamma_3{}^3{}_D$ is due to cascade from 4^3F.

We have likewise made some estimates of cascade for the hydrogen states. By assuming all magnetic quantum number substates for a given principal quantum number to be equally populated, by using the transition probabilities of Wiese et al.,[30] and by considering the experimental emission coefficients for Balmer alpha (n = 3 to n = 2), beta (n = 4 to n = 2), and gamma (n = 5 to n = 2) (given in Table 4), we make the following conjectures: (1) cascade from n = 4 to n = 3 is possibly 13% of the quoted

value for $\gamma_{n=3 \text{ to } n=2}$; (2) cascade from n = 5 to n = 3 is possibly 3% of the quoted value for $\gamma_{n=3 \text{ to } n=2}$; and (3) cascade from n = 5 to n = 4 is possibly 28% of the quoted value for $\gamma_{n=4 \text{ to } n=2}$.

In the only state for which we have accurately determined cascade (He 3^3P) we see that the process of cascade does not dominate direct excitation. Furthermore, from all available evidence, we find that cascade has the same functional dependence on energy as the levels which it populates. Thus the functional dependence on energy of emission coefficients is not greatly influenced by cascade, and emission coefficients may be assumed proportional to excitation coefficients. This assumption is used in Chapter V, where the experimental emission coefficients presented in this chapter are compared with our prediction of excitation coefficients.

There are no published data with which these absolute emission coefficients may be compared. We will show graphically in Chapter V the 10-30 keV energy dependence of the emission coefficient for the He I transition $3^3D \rightarrow 2^3P$ induced by He^+ incidence on Cu at an angle of 45^o; we will also present some earlier, relative data of Kerkdijk and Thomas[1] for the energy range 3.5 - 10 keV, which we normalize to our absolute measurements at 10 keV; the smoothness with which the two sets of data join together lends support to our measurements. We would also note the work of Sterk et al.[8] which measured absolutely the emission coefficient for the Lyman alpha transition induced by proton impact on Al. The coefficient was found to be of the order 10^{-3} photons per proton and was a decreasing function of impact energy in the region 10-30 keV.

From Tables 1-4 we make the observation that only a small fraction of the projectiles produce photon emission. Most excited atoms do in fact

decay by non-radiative mechanisms so that the emission coefficient represents only a small proportion of the atoms which were originally excited. It is of interest to estimate what fraction of the backscattered atoms were excited at the point of emergence from the surface; this can only be calculated very roughly. Let us take as an example the case of 25 keV H^+ incident on molybdenum at 60^o to the surface normal. Summing the emission function of the first three Balmer lines (Table 4) we find the total emission of photons to be 1.9×10^{-4} per incident ion. Using our prediction of total line intensity (as will be explained in the next chapter), we estimate that only 21% of all excited atoms in the n = 3, 4, and 5 levels do in fact radiate and the remaining 79% decay by non-radiative mechanisms; thus the total flux of excited atoms formed in these states is about 8.9×10^{-4} per incident ion. Now, it is clear that this figure does not represent all excited atoms since we do not detect formation of the n = 2 levels. The work of Sterk et al.[8] suggests that formation of n = 2 levels occurs with about the same likelihood as formation of all the higher excited levels combined. Thus the formation of excited recoil atoms occurs for only a few projectiles in every 10^3 that are incident on the surface. The conclusion that is to be drawn from these very rough estimates is that less than 1% of all incident projectiles recoil as excited atoms. Inevitably this means that most backscattered projectiles in this case are either ground state neutrals or ions. A similar conclusion can be drawn from analysis of the case of He^+ impact.

Emission from Sputtered Atoms

For the case of He^+ impact on Al (the lightest element which we

have used as a target), we observe spectral lines characteristic of excited, sputtered Al. These lines do not appear to be Doppler-broadened, indicating rather slow-moving atoms. We have investigated the energy dependence of the emission coefficients for two of these lines, and find them to be a decreasing function of primary energy (Figure 7). We have also observed Al lines in the case of H^+ impact, but only for large angles of incidence (75 degrees). The two lines considered in Figure 7 are the only decay paths of the 4^2S level; adding the two coefficients and subtracting cascade population will give the excitation coefficient of the 4^2S level. Cascade from n = 5 levels contributes about 22% of the excited state population; cascade from higher levels is negligible. This gives an estimate for the 4^2S level excitation coefficient of 1.43×10^{-4} excited Al atoms per incident ion; this is for 25 keV He^+ ion impact at an angle of 45^o. The two lines observed, 3944 Å ($4^2S \rightarrow 3^2P^o$, $J = \frac{1}{2} \rightarrow J = \frac{1}{2}$) and 3962 Å ($4^2S \rightarrow 3^2P^o$, $J = \frac{1}{2} \rightarrow J = 1\frac{1}{2}$), account for all radiative transitions out of the 4^2S level. According to published transition probabilities,[30] the fraction of all transitions represented by the former line is 33%, and by the latter 67%. Using our experimental intensities we find them to be 35% and 65%, respectively.

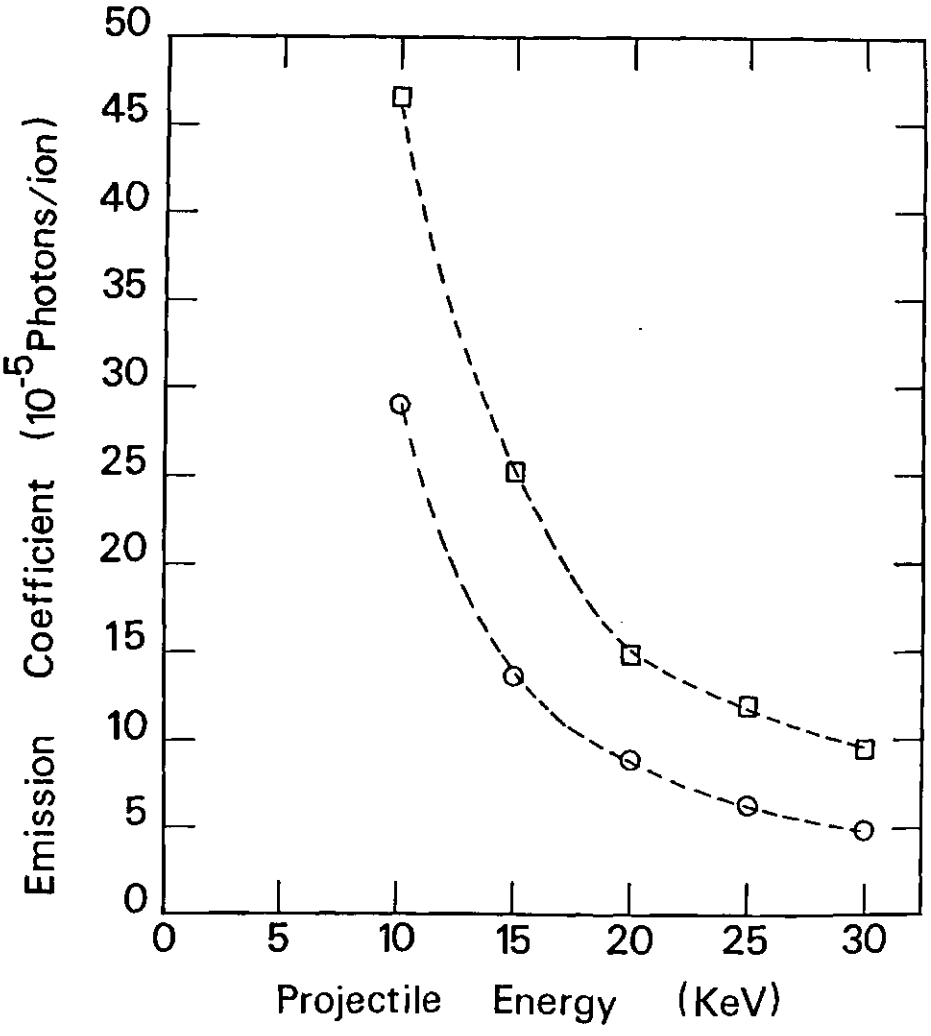

Figure 7. Energy Dependence of Emission from Aluminum. (Emission coefficient of lines from excited sputtered Al as a function of primary energy of He^+ ions (incident at 45^o). Squares, experimental data points for Al-3962 Å ($4^2S \rightarrow 3^2P^o$, $J = \frac{1}{2} \rightarrow J = 3/2$). Circles, experimental data points for Al-3944 Å ($4^2S \rightarrow 3^2P^o$, $J = \frac{1}{2} \rightarrow J = \frac{1}{2}$). The dashed line is drawn to indicate the general trend of the data.

CHAPTER IV

ANALYSIS OF LINE SHAPE

Introduction

In order to predict the shape of the observed Doppler-broadened spectral lines from backscattered particles, and to improve upon the surface-scattering model of Kerkdijk and Thomas[1]; we used the theory of McCracken and Freeman[2] together with the radiationless de-excitation probability given in Equation 4. We present first a descriptive outline of the prediction, to be followed in the next two sub-headings by a detailed mathematical presentation.

The theory of McCracken and Freeman[2] predicts the flux and velocity distribution of all projectiles emerging from the surface into a particular direction; it assumes that the projectile penetrates into the target, losing energy by electronic stopping and suffering no appreciable deviation; at some point it suffers a large-angle deflection by collision with a single target nucleus and is able to return to the surface. This large-angle scattering event is assumed to be governed by a Rutherford scattering expression appropriate to the interaction of the target and projectile nuclei. Based on this picture one may formulate an expression for the probability, dq, that a projectile will emerge with a given energy and direction.

Without any information on the proportion of the scattered projectiles which might be neutralized into a specific excited state, we make

the assumption that this proportion, F, is independent of the emergent particles' energy and direction. As we shall see, some of our work tends to support this assumption. The final factor we must account for is the probability that an excited particle will escape from the influence of the surface without undergoing radiationless de-excitation. This is given by Equation 4, $p(V_{\perp})$. The excited particles that escape will eventually decay radiatively and a certain fraction, F', dependent only on apparatus geometry, will be detected.

Thus, by taking the product of these various quantities (dq, F, $p(V_{\perp})$, and F'), we have the probability of detecting a photon from an emergent particle of given energy and direction. The wavelength of the photon can be simply calculated by the Doppler-shift formula; the non-relativistic form is adequate at the energies used here. This method permits a calculation of the relative line shape if the ratio A/a is known (i.e. in $p(V_{\perp})$). Since in practice this survival coefficient is unknown, we perform the line shape calculation (by numerical integration) for various trial values, and a best fit to experimental data is achieved; from this we establish a "measured" value of A/a.

In addition to the photons which are received directly by the observer, it is possible for an excited atom to emit a photon towards the metal target which then reflects to the observer. Although values of reflectance for polished surfaces are given in standard tables, visual observation shows that the metal surface becomes pitted by the ion bombardment, thus altering the reflectance of the surface. To accommodate this we regard the reflectance as unknown and vary this also to give a best fit to the experimental data. Because the reflected emission has a

trajectory which is opposite to that of the blue-shifted direct emission, reflected photons contribute significantly only to the red-shifted component of the line, whereas the derived value of the survival coefficient A/a is related to the position of the intensity maximum in the blue shift.

We also take into account the influence of monochromator resolution; generally this was kept at 8 Å for He line shapes and at 16 Å for H line shapes. Because, at any given energy, the velocity and Doppler shift of an H atom is twice that of an He atom (in the same trajectory) our doubling of the monochromator resolution for the study of H line shapes kept the ratio of resolution to line width about constant. Because this resolution is comparable to the width of the spectral line, our predicted line shapes have been convoluted with the triangular bandpass characteristic of the monochromator so that this is taken into account in fitting the calculated curve to the experimental data.

Detailed Description of the Model

We now present a detailed description of the model which we have used to predict the shape of Doppler-broadened spectral lines emitted by backscattered particles. Let symbols be defined as follows.

Z_1 = atomic number of ion

m_1 = atomic mass of ion

Z_2 = atomic number of target atom

m_2 = atomic mass of target atom

e = electronic charge

n = density of nuclei in target

a_o = Bohr radius

E^1 = energy at which ion velocity equals velocity of electron in first Bohr orbit

E_o = initial (primary) ion energy

E_c = energy of ion just before collision

E_s = energy of scattered ion as it returns to surface

ξ_c = distance in solid traveled by ion to collision site

ξ_ℓ = distance to surface traveled by backscattered ion away from collision site

ϕ = angle between path of incidence and surface normal (angle of incidence)

θ = angle between path of incidence and path of scattering (scattering angle)

ψ = angle between planes defined by (1) the path of incidence and the path of scattering and (2) the path of incidence and the surface normal (azimuthal angle)

N,N' = normals to surface of solid

$\nu(\xi_c)$ = total number of beam ions at depth ξ_c

λ_o = unshifted wavelength of a photon

λ = observed wavelength of a photon (including shift)

c = speed of light

α = angle between the direction of velocity of the scattered particle and the direction to the observer M

μ = angle between the direction to the observer M and the direction of incidence

M represents the observer (monochromator)

M' represents the reflection of the observer in the metal surface

U represents the incoming beam of ions

W represents the path of a scattered ion

W' represents the projection of W in the plane defined by the incident beam U and the normal to the surface N

The following four figures illustrate the scattering problem and detection problem. Figure 8 is a three-dimensional view; Figure 9 is a two-dimensional view of the plane defined by the paths of incidence and scattering. Figure 10 is a two-dimensional view of the plane defined by the path of incidence and the normal to the surface (the x-z plane), and Figure 11 is a two-dimensional view of the x-z plane showing the direction to the monochromator M. A brief description of the scattering process follows.

An ion (contained in U) of initial energy E_o is incident on the metal surface at O. It penetrates the metal to a depth ξ_c and, in doing so, loses energy by electronic stopping. At point C (within the metal), the ion has energy E_c just before collision with one of the target nuclei. The collision is governed by the cross section $\sigma(E_c, \theta)$, and the energy of the ion after the collision is R^2E_c, where R is given by the usual expression for elastic collisions calculated from conservation of energy and momentum (see Equation (12)). The ion is scattered through an angle θ and loses energy again to the target electrons as it travels the distance ξ_ℓ to the surface, emerging finally at B with energy E_s in the direction denoted by W. Thus, for the ion in the solid, two kinds of collision phenomena are recognized: a single collision of the ion with one of

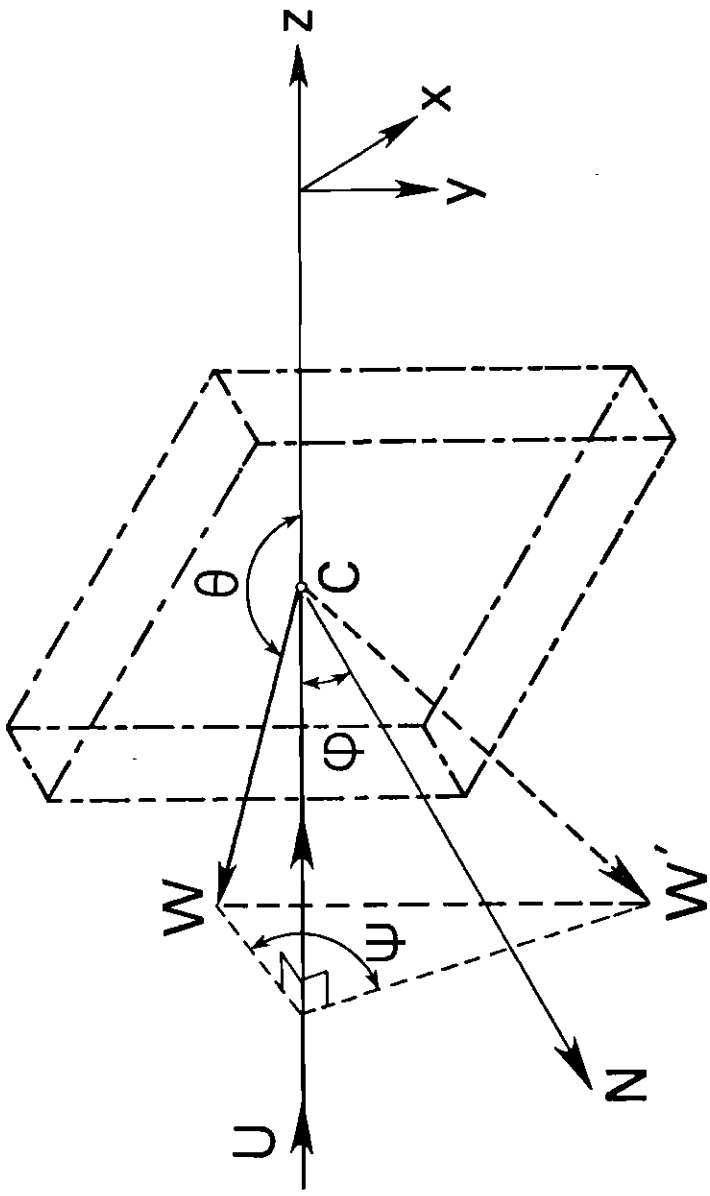

Figure 8. A Three-Dimensional View of the Scattering Problem

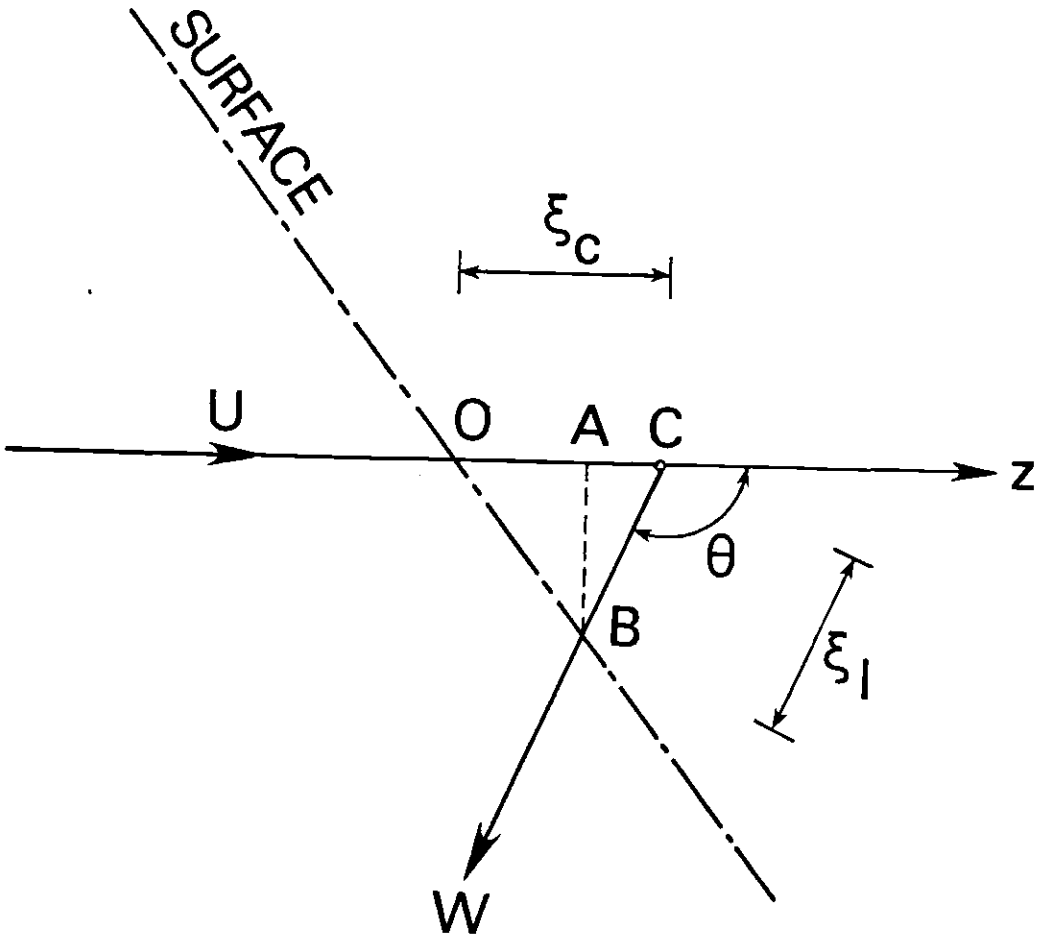

Figure 9. A Two-Dimensional View of the Plane Defined by the Paths of Incidence and Scattering

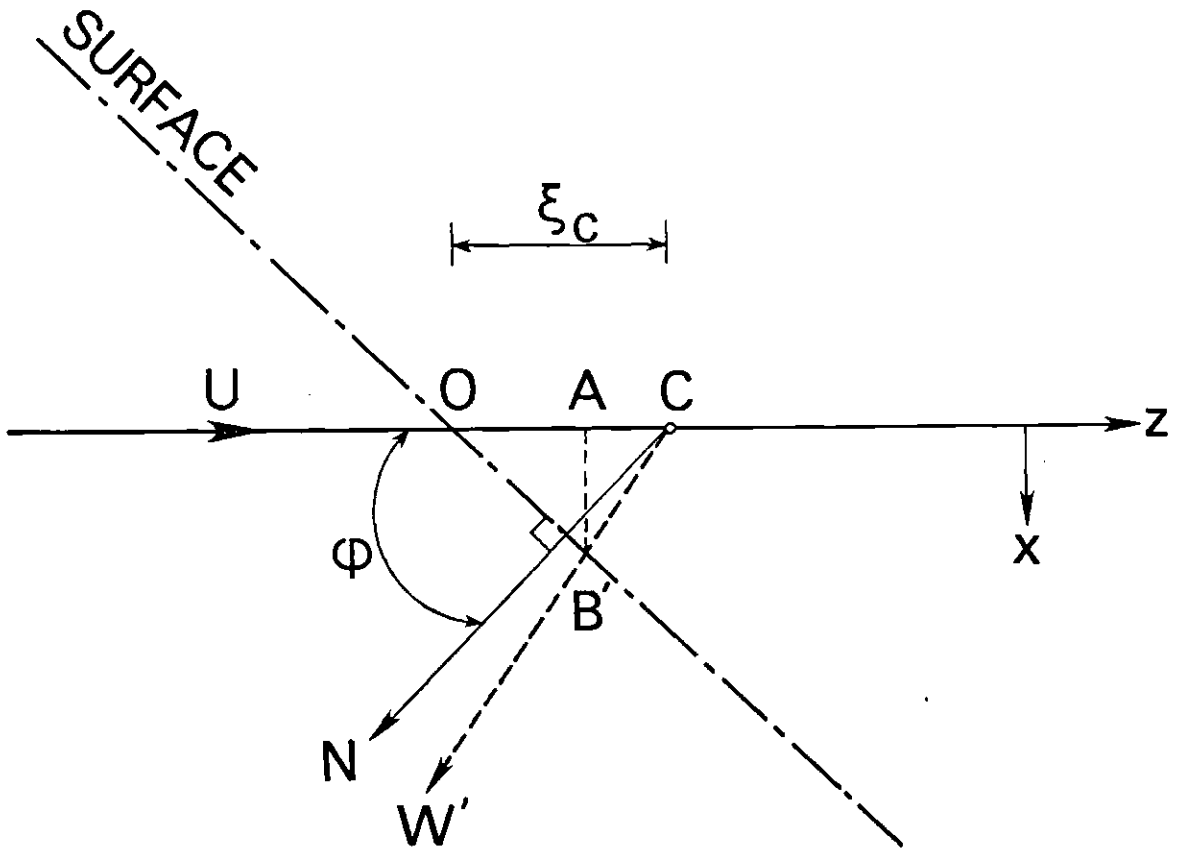

Figure 10. A Two-Dimensional View of the Plane Defined by the Path of Incidence and the Normal to the Surface (the X-Z Plane)

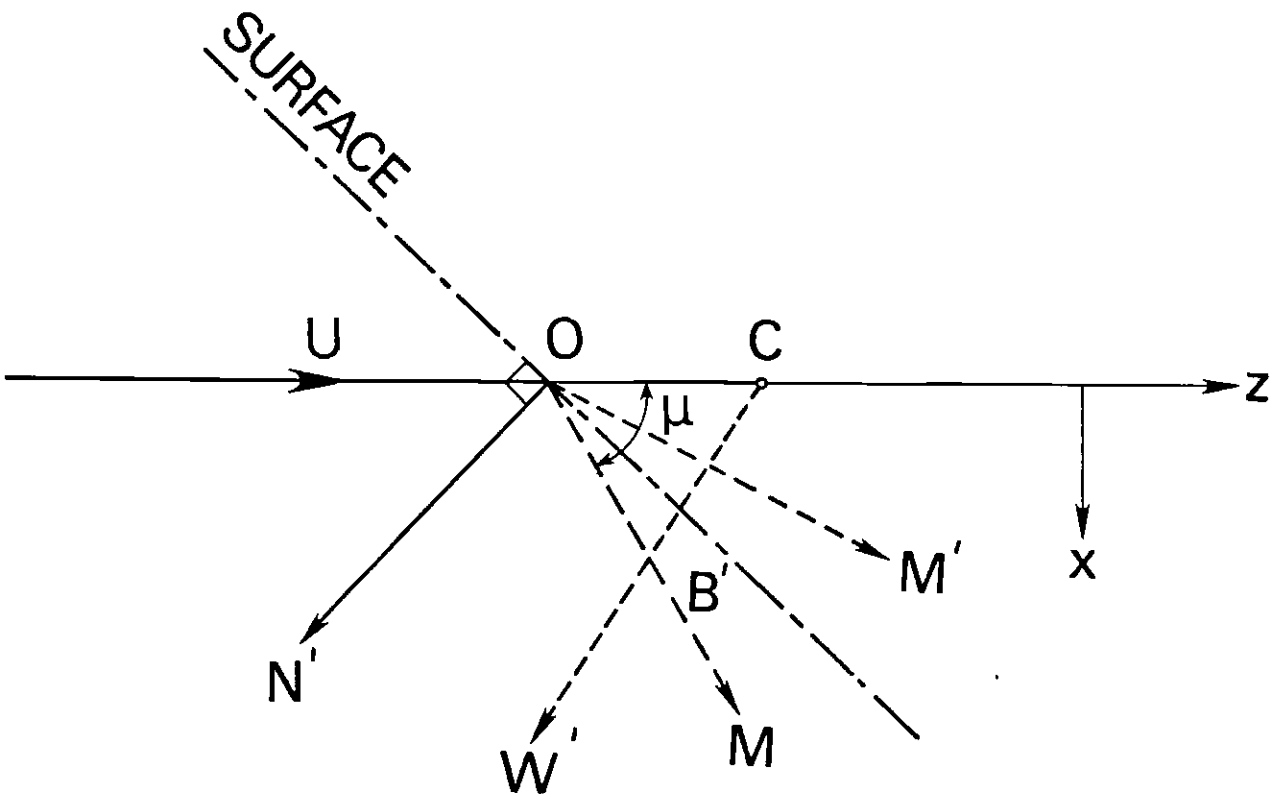

Figure 11. A Two-Dimensional View of the X-Z Plane Showing the Direction to the Monochromator M

the target nuclei and multiple collisions of the ion with the target electrons.

According to McCracken and Freeman,[2] and to Lindhard and Scharff,[32] an ion incident upon a solid target loses energy to the target electrons at a rate given by

$$\frac{dE}{d\xi} = -Z_1^{1/6}\frac{Z_1 Z_2}{(Z_1^{2/3}+Z_2^{2/3})^{3/2}}\, 8\pi n e^2 a_0 \left(\frac{E}{E^1}\right)^{1/2} = -KE^{1/2} \qquad (8)$$

This is known as electronic stopping. From Equation (8) we obtain the energy of the ion for any distance ξ traveled within the solid

$$E(\xi) = \left(\sqrt{E_0} - \tfrac{1}{2} K \xi\right)^2 \qquad (9)$$

In particular, for an ion of initial energy E_o which has penetrated to a depth ξ_c (before undergoing a collision with a target nucleus), we have an expression for the remaining energy (before collision)

$$E_c = E(\xi_c) = \left(\sqrt{E_0} - \tfrac{1}{2} K \xi_c\right)^2 \qquad (10)$$

Thus the cross section governing the collision will be a function of E_c and of the scattering angle θ: $(\sigma(E_c, \theta)$. Furthermore, if $\nu(\xi_c)$ is the total number of beam ions at depth ξ_c, then the number of ions $d\nu$ scattered into the element of solid angle $d\omega$ from the depth range ξ_c to $\xi_c + d\xi_c$ will be given by

$$d\nu = -\nu(\xi_c)\, n\, \sigma(E_c, \theta)\, d\omega\, d\xi_c$$

where $d\omega = \sin\theta\, d\theta\, d\psi$. The negative sign indicates the decrease in beam flux with depth of penetration due to loss by scattering. This equation may be rewritten to give the probability of a scattering event within the depth range ξ_c to $\xi_c + d\xi_c$ into the solid angle $d\omega$:

$$dq = \frac{d\nu}{\nu} = -n\,\sigma(E_c, \theta)\, d\omega\, d\xi_c \tag{11}$$

In the collision the ion will have a discrete energy loss and will then continue to lose energy at a rate given by Equation (8) until it reaches the surface.

We would like to relate E_o (the ion's initial energy), E_c (its energy just before collision), E_s (its energy on returning to the surface), and ξ_c (its path length to the collision site) together with the angles of incidence, scattering, and azimuth. By doing this, we can express the probability given by Equation (11) as a function of E_s and ω (that is, the emergent particle's energy and direction): $dq\ (E_s, \omega)$. McCracken and Freeman calculate Equation (11) for the case of normal incidence and scattering in a single plane. We have generalized their derivation to include non-normal incidence and scattering in three dimensions.

We will denote the energy remaining after the collision by $R^2 E_c$, where R is given by the usual expression for elastic collisions calculated from conservation of energy and momentum:

$$R = \frac{m_1 \cos\theta + \left(m_2^2 - m_1^2 \sin^2\theta\right)^{1/2}}{m_1 + m_2} \tag{12}$$

The path length <u>from</u> the scattering site to the surface, designated ξ_ℓ, can be expressed in terms of the path length <u>to</u> the scattering site ξ_c (see figures).

$$\xi_c = OA + AC$$

$$\begin{aligned} OA &= B'A \cot\angle B'OA \\ &= BA \cos\psi \cot(90^\circ - \phi) \\ &= \xi_\ell \sin(180^\circ - \theta)\cos\psi \tan\phi \\ &= \xi_\ell \sin\theta \cos\psi \tan\phi \end{aligned}$$

$$AC = \xi_\ell \cos(180^\circ - \theta) = -\xi_\ell \cos\theta$$

$$\xi_c = \xi_\ell [\sin\theta \cos\psi \tan\phi - \cos\theta]$$

and

$$\xi_\ell = \frac{\xi_c}{\sin\theta \tan\phi \cos\psi - \cos\theta} = \frac{\xi_c \cos\phi}{\sin\theta \sin\phi \cos\psi - \cos\theta \cos\phi} \tag{13}$$

Using this we can find a relationship between ξ_c and E_s. We have from Equation (9),

$$E_s = \left\{\sqrt{R^2 E_c} - \tfrac{1}{2} K \xi_\ell\right\}^2 \tag{14}$$

and

(Equation (10)) $$E_c = \left\{\sqrt{E_o} - \tfrac{1}{2} K \xi_c\right\}^2$$

so that

$$E_s = \left\{ R\sqrt{E_o} - \tfrac{1}{2} K R \xi_c - \tfrac{1}{2} K \xi_\ell \right\}^2$$

and

$$\sqrt{E_s} = R\sqrt{E_o} - \tfrac{1}{2} K R \xi_c - \tfrac{1}{2} K \xi_\ell$$
$$= R\sqrt{E_o} - \tfrac{1}{2} K R \xi_c - \tfrac{1}{2} K \frac{\xi_c \cos\phi}{\sin\theta \sin\phi \cos\psi - \cos\theta \cos\phi}$$

Solving for ξ_c, we get

$$\xi_c = \frac{2\left\{R\sqrt{E_o} - \sqrt{E_s}\right\}}{K\left\{R + \dfrac{\cos\phi}{\sin\theta \sin\phi \cos\psi - \cos\theta \cos\phi}\right\}} \tag{15}$$

$$= \frac{2\left\{R\sqrt{E_o} - \sqrt{E_s}\right\}}{K\left\{R - \dfrac{\cos\phi}{\cos\theta \cos\phi - \sin\theta \sin\phi \cos\psi}\right\}}$$

and

$$d\xi_c = -\frac{1}{K\sqrt{E_s}} \frac{dE_s}{\left\{R - \dfrac{\cos\phi}{\cos\theta \cos\phi - \sin\theta \sin\phi \cos\psi}\right\}} \tag{16}$$

We may also determine E_c from Equations (10) and (15).

$$E_c = \left\{\sqrt{E_o} - \tfrac{1}{2} K \xi_c\right\}^2 \tag{17}$$
$$= \left\{\sqrt{E_o} - \tfrac{1}{2} K \frac{2}{K} \frac{\left[R\sqrt{E_o} - \sqrt{E_s}\right]}{\left[R - \dfrac{\cos\phi}{\cos\theta \cos\phi - \sin\theta \sin\phi \cos\psi}\right]}\right\}^2$$

(continued)

$$= \left\{ \frac{\sqrt{E_s} - \dfrac{\sqrt{E_0}\cos\phi}{\cos\theta\cos\phi - \sin\theta\sin\phi\cos\psi}}{R - \dfrac{\cos\phi}{\cos\theta\cos\phi - \sin\theta\sin\phi\cos\psi}} \right\}^2$$

The cross section used in our formulation governs the interaction between the two nuclei. This Rutherford cross section (in Gaussian units) is given by

$$\sigma(E_c,\theta)\,d\omega = \frac{1}{16}\,\frac{Z_1^2 Z_2^2 e^4}{E_c^2}\,\frac{1}{\sin^4\frac{\theta}{2}}\,d\omega \qquad (18)$$

where $d\omega = \sin\theta\, d\theta\, d\psi$.

Using our expression for E_c, Equation (17), we have

$$\sigma(E_c,\theta)\,d\omega = \frac{Z_1^2 Z_2^2 e^4}{16\sin^4\frac{\theta}{2}} \left\{ \frac{R - \dfrac{\cos\phi}{\cos\theta\cos\phi - \sin\theta\sin\phi\cos\psi}}{\sqrt{E_s} - \dfrac{\sqrt{E_0}\cos\phi}{\cos\theta\cos\phi - \sin\theta\sin\phi\cos\psi}} \right\}^4 d\omega \qquad (19)$$

Thus we are finally able to rewrite Equation (11) using the specified quantities.

$$dq(E_s,\omega) = \frac{n Z_1^2 Z_2^2 e^4}{16\sin^4\frac{\theta}{2}} \times \qquad (20)$$

$$\frac{\left\{ R - \dfrac{\cos\phi}{\cos\theta\cos\phi - \sin\theta\sin\phi\cos\psi} \right\}^3}{\left\{ \sqrt{E_s} - \dfrac{\sqrt{E_0}\cos\phi}{\cos\theta\cos\phi - \sin\theta\sin\phi\cos\psi} \right\}^4} \frac{d\omega\, dE_s}{K\sqrt{E_s}}$$

with $d\omega = \sin\theta\, d\theta\, d\psi$.

which represents the total backscattered flux for an element of solid angle and for an element of energy. This equation with ϕ and ψ equal to zero reduces to Equation (7) (page 662) of the paper by McCracken and Freeman.[2]

Recalling the definition of K (Equation (8)), the factor independent of energy and angle in Equation (20) may be rewritten:

$$\frac{n Z_1^2 Z_2^2 e^4}{16K} = \frac{n Z_1^2 Z_2^2 e^4}{16} \frac{(Z_1^{2/3} + Z_2^{2/3})^{3/2}\sqrt{E'}}{Z_1^{1/6} Z_1 Z_2 8\pi n e^2 a_0} \qquad (21)$$

$$= \frac{e^2\sqrt{E'}}{128\pi a_0} Z_1^{5/6} Z_2 (Z_1^{2/3} + Z_2^{2/3})^{3/2}$$

In our prediction of relative line shape this Z-dependent factor is normalized to a constant value (as will be explained in the next subheading).

Because we have no information on the proportion of scattered projectiles which might be neutralized into a specific excited state, we assume that this proportion, F, is independent of the emergent particle's energy and direction.

The final factor we must account for is the probability that an excited particle will escape from the influence of the surface without undergoing radiationless decay. For an emerging particle having a velocity component $V_\perp$ perpendicular to the surface, this probability is[5]

$$p(V_\perp) = \exp(-A/a V_\perp) \qquad (22)$$

It is simply a matter of expressing $V_\perp$ in terms of the angular parameters. From the diagrams we see that the components of V are (since V is directed along the path length ξ_ℓ)

$$V_x = V \sin \angle OCB \cos\psi = V \sin\theta \cos\psi \tag{23}$$

$$V_y = -V \sin \angle OCB \sin\psi = -V \sin\theta \sin\psi$$

$$V_z = -V \cos \angle OCB = V \cos\theta$$

and we have for $V_\perp$

$$V_\perp = V_x \sin\phi - V_z \cos\phi$$

$$= V \sin\theta \sin\phi \cos\psi - V \cos\theta \cos\phi$$

Therefore

$$p(V_\perp) = \exp - \left[\frac{A}{a} \frac{1}{V(\sin\theta \sin\phi \cos\psi - \cos\theta \cos\phi)} \right]$$

or, since

$$V = \sqrt{\frac{2E_s}{m_1}} \quad ,$$

$$p(E_s, \omega) = \exp - \left[\frac{A}{a} \sqrt{\frac{m_1}{2E_s}} \frac{1}{\sin\theta \sin\phi \cos\psi - \cos\theta \cos\phi} \right] \tag{24}$$

These excited particles will eventually decay radiatively and a certain fraction, dependent on apparatus geometry, will be detected. Let us denote by the factor, F', the fraction of (surviving) excited atoms that will give a photon that is detected by the observer. For a given transition, this fraction F' is assumed independent of the speed and direction of the projectiles.

Thus, combining these various terms we have the probability $dP(E_s,\omega)$ of detecting a photon from an emergent particle of energy E_s, scattered into a solid angle $d\omega$, which is (referring to Equations (20) and (24))

$$dP(E_s,\omega) = F' F\, p(E_s,\omega)\, dq(E_s,\omega) \tag{25}$$

The wavelength of the photon can be calculated by the Doppler-shift formula; since our maximum energy has been 30 keV, the non-relativistic form is adequate:

$$\lambda = \lambda_0\left[1 - \frac{V}{c}\cos\alpha\right] \tag{26}$$

where α is the angle between the direction of velocity of the scattered particle and the direction to the observer M (monochromator). As we see in Figure 11, the point of observation is located in the plane which includes the path of incidence and the normal to the surface and is at an angle μ with respect to the positive z-axis. Using the x, y, z components of V (Equation (23)), we can determine the component of V toward the observer, which we represent as V_M:

$$V_M = V_x \sin\mu + V_z \cos\mu$$
$$= V \sin\theta \sin\mu \cos\psi + V \cos\theta \cos\mu$$

Therefore

$$\lambda = \lambda_0 \left[1 - \frac{V}{c}(\sin\theta \sin\mu \cos\psi + \cos\theta \cos\mu\right]$$

or

$$\frac{\lambda_0 - \lambda}{\lambda_0} = \frac{V}{c}\left[\sin\theta \sin\mu \cos\psi + \cos\theta \cos\mu\right] \quad (27)$$

In addition to these directly observed photons, it is quite possible for an excited atom to emit a photon towards the target which then reflects to the observer. We now determine the Doppler-shift for such a reflected photon. Finding the component of velocity toward the observer M for a reflected photon is equivalent to finding the component of velocity toward the reflection of the observer M' (in the metal surface) for a direct photon. We have the x, y, z components of V (Equation (23)); we need to determine their projections toward M' (see Figure 11). This amounts to determining the value of $\angle$ M'OC in terms of angles ϕ and μ.

$$\angle N'OM = 180° - \phi - \mu$$
$$\angle MOB' = 90° - \angle N'OM = 90° - (180° - \phi - \mu)$$
$$= \phi + \mu - 90°$$
$$\angle M'OC = 180° - \phi - \angle N'OM - \angle MOB' - \angle B'OM'$$
$$\angle B'OM' = \angle MOB'$$

so that

$$\begin{aligned}\angle M'OC &= 180^\circ - \phi - (180^\circ - \phi - \mu) - 2(\phi + \mu - 90^\circ) \\ &= 180^\circ - \phi - 180^\circ + \phi + \mu - 2\phi - 2\mu + 180^\circ \\ &= 180^\circ - 2\phi - \mu\end{aligned}$$

therefore

$$\begin{aligned}V_{M'} &= V_x \sin \angle M'OC + V_z \cos \angle M'OC \\ &= V \sin\theta \sin(180^\circ - 2\phi - \mu) \cos\psi \\ &\quad + V \cos\theta \cos(180^\circ - 2\phi - \mu)\end{aligned}$$

and

$$\frac{\lambda_o - \lambda}{\lambda_o} = \frac{V}{c}\left[\sin\theta \sin(180^\circ - 2\phi - \mu)\cos\psi + \cos\theta \cos(180^\circ - 2\phi - \mu)\right] \tag{28}$$

for a reflected photon.

In order to integrate dP (E_s, ω) over all applicable angles ($d\omega$) and energies (dE_s), we must determine the ranges of the angles θ and ψ and of E_s. By symmetry, scattering into negative ψ is the same as scattering into positive ψ; therefore the range of ψ is 0 to 180°. The minimum scattering angle θ_{min} is determined from the path of an ion which collides at the surface to be scattered along the surface. According to Figures 9 and 10

$$\theta_{min} = \angle BOA$$

therefore,

$$\tan\theta_{min} = \frac{BA}{OA} = \frac{B'A}{\cos\psi}\,\frac{1}{OA} = \frac{1}{\cos\psi}\,\frac{B'A}{OA}$$

$$= \frac{1}{\cos\psi}\tan\angle B'OA$$

$$\angle B'OA = 90^\circ - \phi$$

Therefore

$$\tan\theta_{min} = \frac{1}{\cos\psi}\tan(90^\circ - \phi) = \frac{\cot\phi}{\cos\psi} \tag{29}$$

$$\theta_{max} = 180^\circ \tag{30}$$

The maximum recoil energy $E_{s\ max}$ is that which an ion would have after an elastic surface collision; hence

$$E_{S\ max} = R^2 E_o \tag{31}$$

where R is given by Equation (12). The Minimum recoil energy $E_{s\ min}$ is rather arbitrarily taken to be 20 eV; the rationale is that any projectile that has been reduced to this energy will probably be captured by the lattice.

Method of Calculation

Now that the derivation of the model has been explained, we describe the steps taken in making a calculation. We read the following information into the computer:

(1) the atomic masses of the incident and target particles

(2) the primary energy of the incident ions

(3) the angle of incidence

(4) the angle between the direction toward the monochromator and the direction of incidence

(5) a trial value of the reflectance of the surface (ratio of quantity of light reflected to quantity of light incident)

(6) the value of the quantity given in Equation (21) multiplied by F and F', which we take equal to unity. Thus our line shape is evaluated in relative terms only and at the end is given a convenient scale for comparison with the data.

(7) a trial value of the survival coefficient A/a

(8) the true unshifted wavelength of the line (λ_o)

(9) the dispersion of the monochromator

(10) the slit-width of the monochromator

(11) the maximum value of a given set of data (in arbitrary units)

(12) the number of data points being used

(13) the value in arbitrary units of the background intensity level underlying the line

(14) the data points as ordered pairs: intensity at a particular wavelength (arbitrary units), that wavelength as read from monochromator.

First of all, correction is made for the wavelength offset of the monochromator. Then the numerical integration is performed according to the following steps.

(1) The (positive) range of the aximuthal angle ψ (0 to 180^o)

divided into ten-degree steps. The first value ψ_1 (=0) is chosen.

(2) The minimum value of the scattering angle (θ_{min}) is determined from ψ_1 and the (constant) angle of incidence ϕ, according to Equation (29). Then the range for θ, θ_{min} to 180^{o}, is divided into ten-degree steps. The first value θ_1 ($=\theta_{min}$) is chosen.

(3) Using θ_1, the maximum energy of scattered particles is determined from

$$E_{s\ max} = R^2\ E_o \quad \text{(Equation (31))}$$

where R is given by Equation (12). The minimum energy, as stated before, is 20 eV. The energy range 20 eV to $E_{s\ max}$ is divided into 20 parts, and the first value E_{s_1} (=20 eV) is chosen.

(4) Using the angle of incidence and primary energy, and the values ψ_1, θ_1, and E_{s_1}, the relative value of dq (E_s, ω) is calculated using Equation (20).

(5) Using these same angular parameters and E_{s_1}, the exponential survival probability is calculated according to Equation (24). This is then multiplied by the result of step (4) to give a quantity Q.

(6) Using Equation (27), the fractional shift in wavelength for direct emission corresponding to ψ_1, θ_1, and E_{s_1} is calculated, multiplied by 10^4 to put it in convenient form and rounded off to some integer I. Storage registers numbered

-100 through 0 through +100 are set up, and the quantity Q is added to register I.

(7) Using Equation (28), the fractional shift in wavelength for reflected emission corresponding to ψ_1, θ_1, and E_{s_1} is calculated, multiplied by 10^4, and rounded off to some integer J. The product of Q and the trial reflectance are added to register J.

(8) Steps (4) through (7) are repeated for every energy E_s.

(9) Steps (3) through (8) are repeated for every scattering angle θ.

(10) Steps (2) through (9) are repeated for every azimuthal angle ψ. In this way a histogram is built up.

(11) Because the resolution of the monochromator is comparable to the width of the spectral line, the histogram is convoluted with the triangular bandpass characteristic of the monochromator so that this is taken into account in fitting the calculated curve to the experimental data. This is done by using a triangular function of altitude equal to unity and of base equal to twice the product of monochromator dispersion and slit width. The vertex of the triangle is aligned with a particular storage register (as established in step (6)) and a product is made of the two functions, triangle and histogram; the integral of this product becomes the new quantity in the (emptied) storage register. This is done for each storage register of the histogram.

(12) By fitting the calculated curve to a given set of data points,

the values for the survival coefficient and reflectance are determined. Initially three values of survival coefficient are tested, with the original read-in value as midpoint between the other two. For each of these three values a line shape is predicted and a value of reflectance chosen by a least-squares fit to the data points. The one survival coefficient (out of three) which provides the best fit to the data points (i.e. the smallest sum of squared deviations) is chosen for the midpoint of the two new trial values, whose separation is only half that of the initial trial values. For each of these three values a line shape is predicted and a value of reflectance chosen as before. The one value of these three which provides the best fit to the data is selected to be the midpoint of the new reduced (by half) interval. Thus the process continues until ten sets of three values have been tested. The last value selected becomes our determination of survival coefficient. It should be noted that for each value of survival coefficient tested the triangular bandpass function of the monochromator must be re-convoluted into the line shape.

(13) Finally we have a line shape using our best-fit value of survival coefficient and its corresponding best-fit value of reflectance. The maximum value of both the calculated curve and the data points is normalized to unity, with the other values being scaled accordingly, in order to facilitate comparison. The ordinates of the (normalized) histogram

are printed out together with their corresponding fractional wavelength shifts. Also the (normalized) data points are printed, with abscissas converted to fractional wavelength shifts. It might be noted that the calculation has also been made for angular intervals of three degrees and for the energy range divided into 100 parts; no appreciable difference was noted in the line shape predicted.

Results of Line Shape Analysis

The outcome of this calculation is that a line shape is predicted which is of the same form as that observed experimentally. Moreover, with suitable choice of the survival coefficient A/a and surface reflectance one can get very good agreement with the measured line shape. In Figure 12 we show the shape of the 5876 Å line induced by 30 keV He^+ on Nb at an incidence angle ϕ of 60^o; this is compared with the predicted line shape using the surface-scattering model, and with the predicted line shape using the present model. The agreement with the data in the case of the present model is a noticeable improvement over the surface-scattering model. We also show the predicted line shape using the present model with $A/a = 0$; i.e. radiationless decay does not occur and all excited atoms escape and subsequently radiate. Clearly the predicted shape for this situation bears little resemblance to observation. We note that the prediction by the surface-scattering model (which does not include radiationless de-excitation) provides more satisfactory agreement with the data than does the present model excluding radiationless de-excitation (i.e. $A/a = 0$). This implies that most of the excited atoms

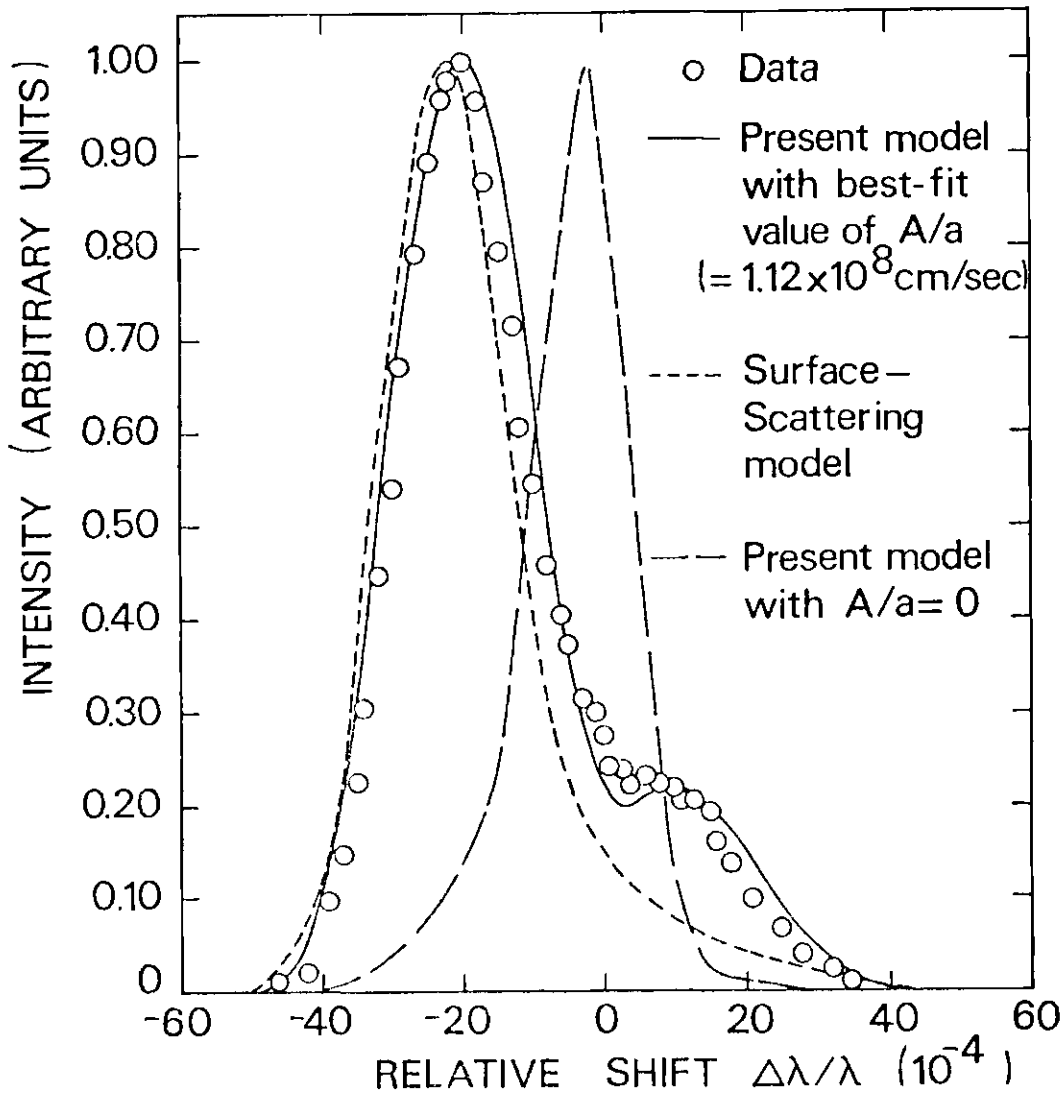

Figure 12. Measured and Predicted Line Shape of the 5876 Å ($3^3D \rightarrow 2^3P$) He I Emission. (Experimental conditions: 30 KeV He^+ incident on Nb at an angle of 60^o. Intensity is shown as a function of relative wavelength shift, defined as the shift ($\Delta\lambda$) from the 5876 Å line divided by the wavelength of that line, 5876 Å (λ).)

which finally radiate are backscattered in surface collisions with a large fraction of their initial energy; thus they are the atoms for which radiationless de-excitation may most accurately be ignored. However, when bulk penetration of the target by the incident ions is included, as it is in the present model, the excited atoms backscattered in collisions below the surface are greatly reduced in energy and therefore especially subject to radiationless de-excitation. Thus the necessity for such a term in our theory. We repeat the "best-fit" curve ($A/a \neq 0$) by the present model in Figure 13, with an indication of the direct and reflected components of the total intensity.

Another example of line shape is given in Figure 14, which shows the agreement between theory and experiment for the 6563 Å (n = 3 to n = 2) H_α line induced by 25 keV H^+ impact on Mo at 60° incidence. We find that for large angles of incidence ($\phi \geq 45^\circ$) the fit to the line shape is quite sensitive to the choice of survival coefficient. For these angles we believe that the survival coefficient can be determined to an accuracy of ± 25%; varying the survival coefficient by this amount from the "best-fit" value can shift the wavelength at which maximum intensity occurs by as much as 2 Å and produces clearly inferior agreement with the experimental data. For small incidence angles ($\phi < 45^\circ$) the fitting of calculated and measured line shapes becomes progressively less sensitive to the choice of survival coefficient; in addition, the reduced backscattered flux at these angles results in lower signal strengths; thus we consider that the accuracy with which A/a may be established is poor for incidence angles below 45°. Therefore the values of survival coefficient quoted here are derived for incidence angles $\phi \geq 45^\circ$.

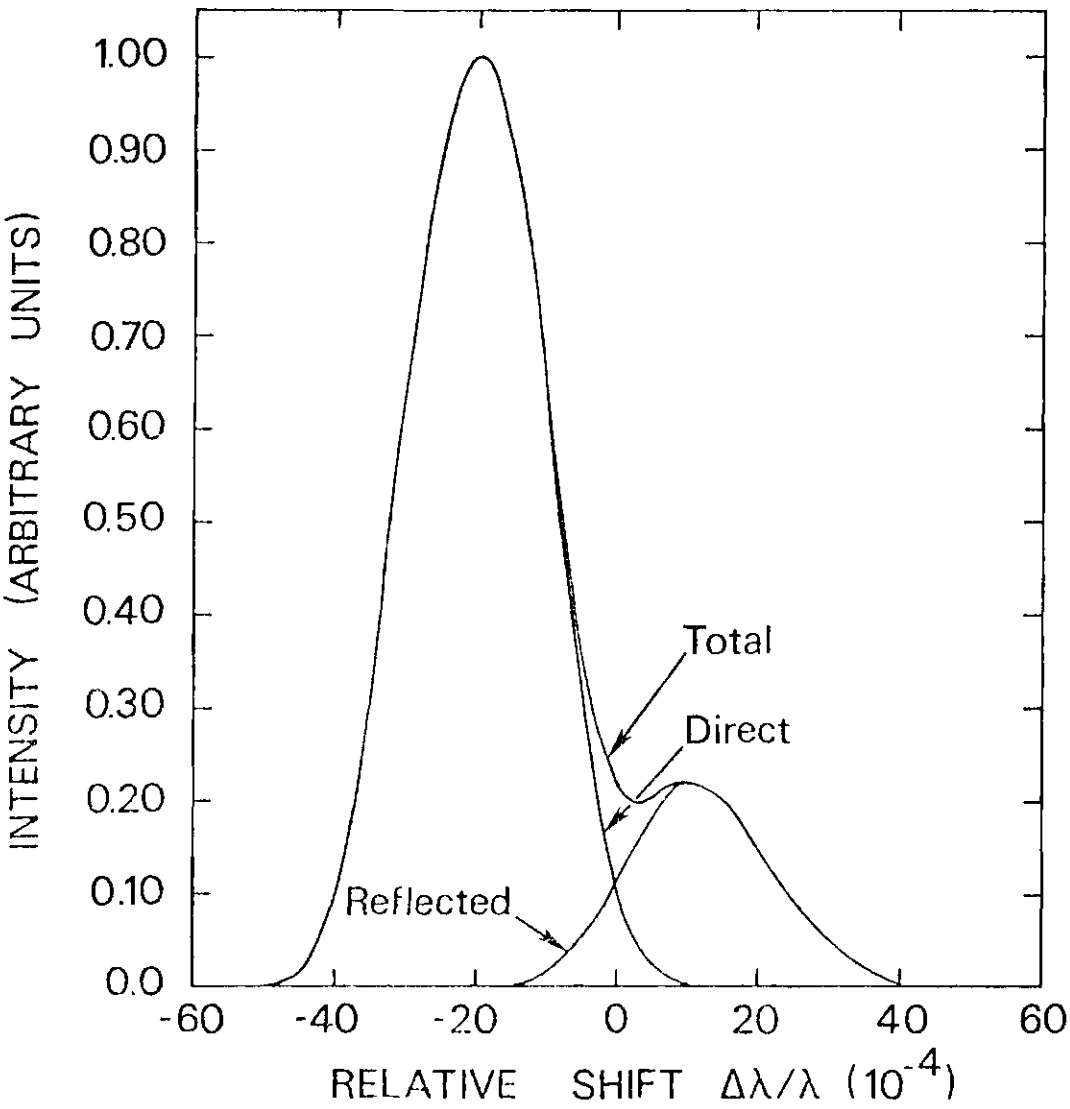

Figure 13. Predicted Shape of the He I 5876 Å Line Showing Direct, Reflected, and Total Emission Intensity. (The calculation has been made for 30 KeV He^+ incident on Nb at an angle of 60^o. The survival coefficient A/a is taken to be 1.12×10^8 cm/sec, and the surface reflectance 0.22. (This is the solid curve of Figure 12.))

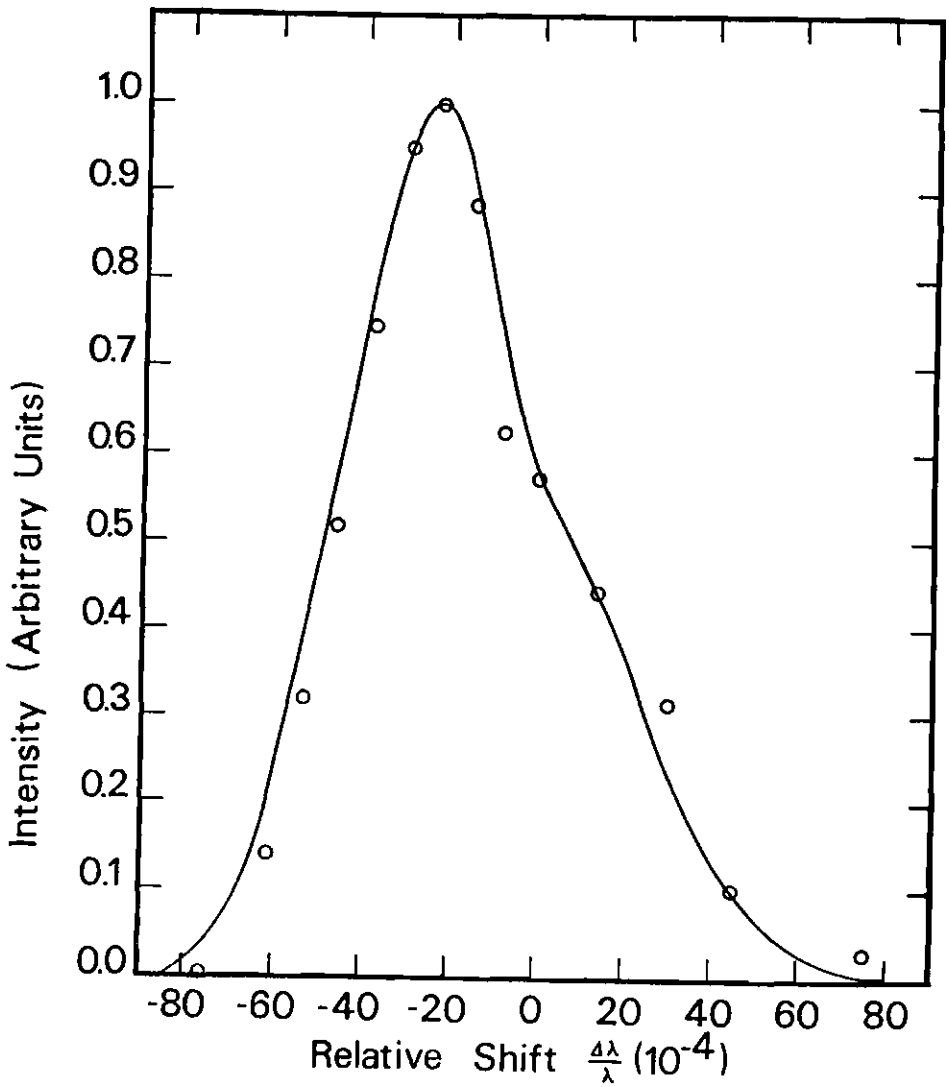

Figure 14. Measured and Predicted Line Shape of the 6563 Å (n = 3 to n = 2) H Emission. (Experimental conditions: 25 KeV H^+ incident on Mo at an angle of 60^o. Circles, experimental data points; solid line, prediction by our model with survival coefficient chosen for best fit to data points (A/a = 7.2 x 10^7 cm/sec).)

In a particular case (30 keV He^+ on Nb) we have shown that a derived value (for $\phi \geq 45^o$) is consistent with the experimental data for lower angles of incidence.

The survival coefficient, A/a, for the 3^3D state of He as determined from the 5876 Å He I emission for the cases of Cu, Nb, and Mo targets, was found to be, respectively, 3.0×10^8, 1.3×10^8, and 1.0×10^8 cm/sec. The survival coefficients for the 4^3D state of He as determined from the 4472 Å line shape for the cases of Cu and Nb targets were, respectively, 1.6×10^8 and 0.8×10^8 cm/sec. Finally, the survival coefficient for the 3^3P state, derived from the 3889 Å line shape in the single case of an Nb target, was found to be 1.5×10^8 cm/sec. In all cases these values are the means of several determinations at different energies and impact angles; there was no apparent systematic variation with energy or angle. Thus using the interpretation of A/a as a critical normal velocity component, we see that backscattered 3^3D He atoms must have a greater normal velocity away from an Nb surface than from an Mo surface in order to have the same probability of escape, and a still greater normal velocity away from a Cu surface. Also, for an Nb target, backscattered He atoms in the 3^3D state must have a greater normal velocity component than those in the 4^3D state; those in the 3^3P state must have a still greater normal velocity. The other cases may be compared similarly.

The determinations of survival coefficient for the n = 3 state of H, derived from analysis of the Balmer alpha line shape, yield a mean value of 7.8×10^7 cm/sec for the three metals considered, Cu, Nb, and Mo. The observed variation among metals is less than the statistical relia-

bility of the data. For the excited states studied, we see that an excited He atom recoiling from Cu, Nb, or Mo requires a greater normal velocity component than an excited H atom in order to have the same probability of escape.

We have also studied the line shape of the Balmer alpha line induced by H_2^+ impact on Mo and find it to be exactly the same as the corresponding situation for H^+ impact at the same velocity. This suggests that the H_2^+ ion dissociates at impact on the surface, and the fragments are uncorrelated in their subsequent behavior.

In order to test the applicability of the Rutherford scattering cross section to our analysis, we have performed some calculations of line shape in which we replace the Rutherford expression with a screened-coulomb cross section as formulated by Everhart et al.[33] This change tends to provide a less satisfactory fit of our predicted curve to the experimental data and a survival coefficient which is within 50% of our stated value. Figure 15 shows an example of this calculation together with the experimental data (as in Figure 14).

Our explanation of the poorer fit provided by the screened-coulomb cross section lies in its limited applicability to metallic atoms in a crystalline solid. A screened-coulomb cross section properly applies to an isolated, neutral atom, whose unperturbed electron shells screen the electric field of the positively charged nucleus. In the case of a polycrystalline metal, the valence electrons are free to move about; thus static screening is supplied only by the inner electron shells, with the mobile valence electrons keeping the metal as a whole neutral. Thus screening takes place, but not of the particular kind for which a typical

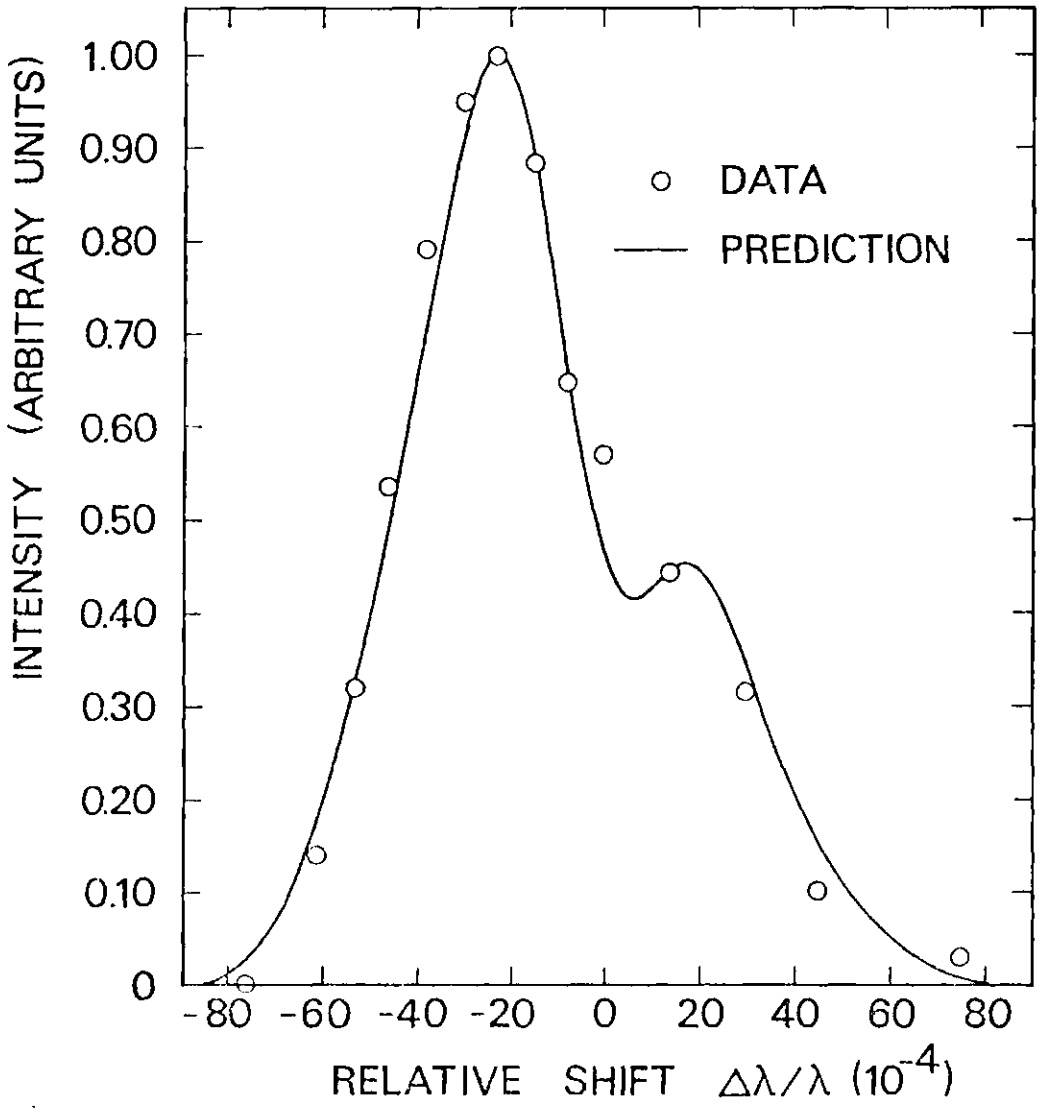

Figure 15. Screened-Coulomb Prediction of the 6563 Å H Line Shape. (Comparison is made with data. Experimental conditions: 25 KeV H^+ incident on Mo at an angle of 60°. By this prediction $A/a = 1.11 \times 10^8$ cm/sec.)

screened-coulomb cross section applies.

For purposes of comparison we now present the values of survival coefficient arrived at by a number of workers (as mentioned in Chapter I). Janev et al.[22] perform theoretical calculations for Li^+, Li, and Na^+ impact on Mo and W; for resonance processes they derive values of A/a from 3.2×10^{11} cm/sec to 1.5×10^{13} cm/sec. Because these are heavier metallic projectiles (in contrast to H^+ and He^+), the relevance of these values to our work is questionable. Gersten and Tzoar[21] derive a value of $A/a = 6.12 \times 10^7$ cm/sec for the case in which the energy released in a Lyman beta transition (for an H atom at an Al surface) excites a surface plasmon emission, instead of creating a photon. Because this type of de-excitation may be in competition with other radiationless processes, the value of A/a determined by experiment may differ considerably from this value, depending on the relative strengths of the various de-excitation processes. Somewhat more applicable to our work are the theoretical values of Cobas and Lamb[20] and of Shekhter[19] as interpreted by Hagstrum.[3] For resonance processes the survival coefficient A/a predicted by Shekhter[19] for protons at an Mo surface is 1.8×10^{11} cm/sec and that predicted by Cobas and Lamb[20] for He^+ at an Mo surface is 4.8×10^{10} cm/sec. These values are three orders of magnitude higher than our measurements. For Auger de-excitation of $He(2^3S)$ at an Mo surface Cobas and Lamb[20] predict $A/a = 1.3 \times 10^8$ cm/sec which is quite comparable with the measurements of A/a which we present here. Because Cobas and Lamb[20] use hydrogenic wavefunctions for He particles, their results are expected to be only order of magnitude determinations.

The values of A/a determined experimentally include 2×10^6 cm/sec for sputtered, excited Cu atoms at a Cu surface as established by van der Weg and Bierman,[5] and by White and Tolk[13]; they make no effort to ascertain the dominant radiationless process. Because this determination involves sputtered, rather heavy atoms, it is not particularly relevant to our work. Of more relevance is the value given by Smits[23] and Kerkdijk[24] of $A/a = 1.5 \times 10^8$ cm/sec for the $n = 4$ state of H, as determined from the Balmer beta ($n = 4$ to $n = 2$) H emission, induced by 10-40 keV protons incident on Cu. Again no attempt is made to ascertain the dominant radiationless process. We do not present measurements for this particular state of H, but observe that this value is also comparable with those that we present.

CHAPTER V

THE PREDICTION OF EXCITATION COEFFICIENTS

Dependence of Coefficients on Angle and Energy

The general relationship between emission and excitation coefficients, as stated in Chapter III (Equation 5), is given by

$$\gamma_{jK} = \left\{ \gamma_j + \sum_{i>j} \gamma_{ij} \right\} \times \frac{A_{jK}}{\sum_{K<j} A_{jK}}$$

In Chapter III, we further explain that on the basis of all available evidence it is reasonable to assume that emission coefficients are proportional to excitation coefficients. We have made measurements of emission coefficients and have determined their absolute magnitudes by calibrating our detection system; these values have been tabulated in Chapter III. In order to predict corresponding excitation coefficients, we have used our model of line shape: a line shape is predicted and then integrated over all wavelengths to provide a relative measure of excitation coefficient. By repeating the integration of the predicted line shape for various impact energies and angles of incidence, we arrive at the functional dependences of the excitation coefficient on these two parameters. We may then compare our experimental emission coefficients with these predicted dependences.

Two important parameters are unknown in our model for predicting line shape and excitation coefficient. We have no theoretical knowledge

of the survival coefficient A/a; however, we have our experimentally obtained (best-fit) values given in Chapter IV, and we can use these for the prediction. Secondly, we have no information on the probability that a backscattered atom will be excited; this is the factor F in Equation 25. For the purpose of this calculation, we continue to make the assumption that this factor is independent of the emergent particle's energy and direction; success of the predictions would tend to confirm the validity of the assumption. We make no assumption as to the magnitude of this factor, and so our predictions will indicate relative variations only; we therefore normalize theory to experiment to perform a comparison.

We do again note that the measured quantity is an emission coefficient γ_{jk}, and the predicted quantity is an excitation coefficient γ_j; our discussion in Chapter III suggests that these two quantities are proportional to each other. Thus a comparison of the measured γ_{jk} with the predicted γ_j is valid.

In Figure 16 we show a predicted angular dependence normalized to the experimental data for the case of 25 KeV protons incident on Nb; the agreement between prediction and experiment is within the statistical variation of our data (± 6%) except at 60^{o}. No explanation is given for this single discrepancy. Similarly, for the case of 30 KeV He^{+} incident on Nb, we show in Figure 17 a predicted angular dependence compared with experimental data; in this case the emission coefficient data have not been put on an absolute scale and are expressed in arbitrary units; the two sets of relative values (theory and experiment) have been normalized together at one point. The predicted curve in this case shows an average absolute percent deviation from the data of 23%; the deviation in this case appears

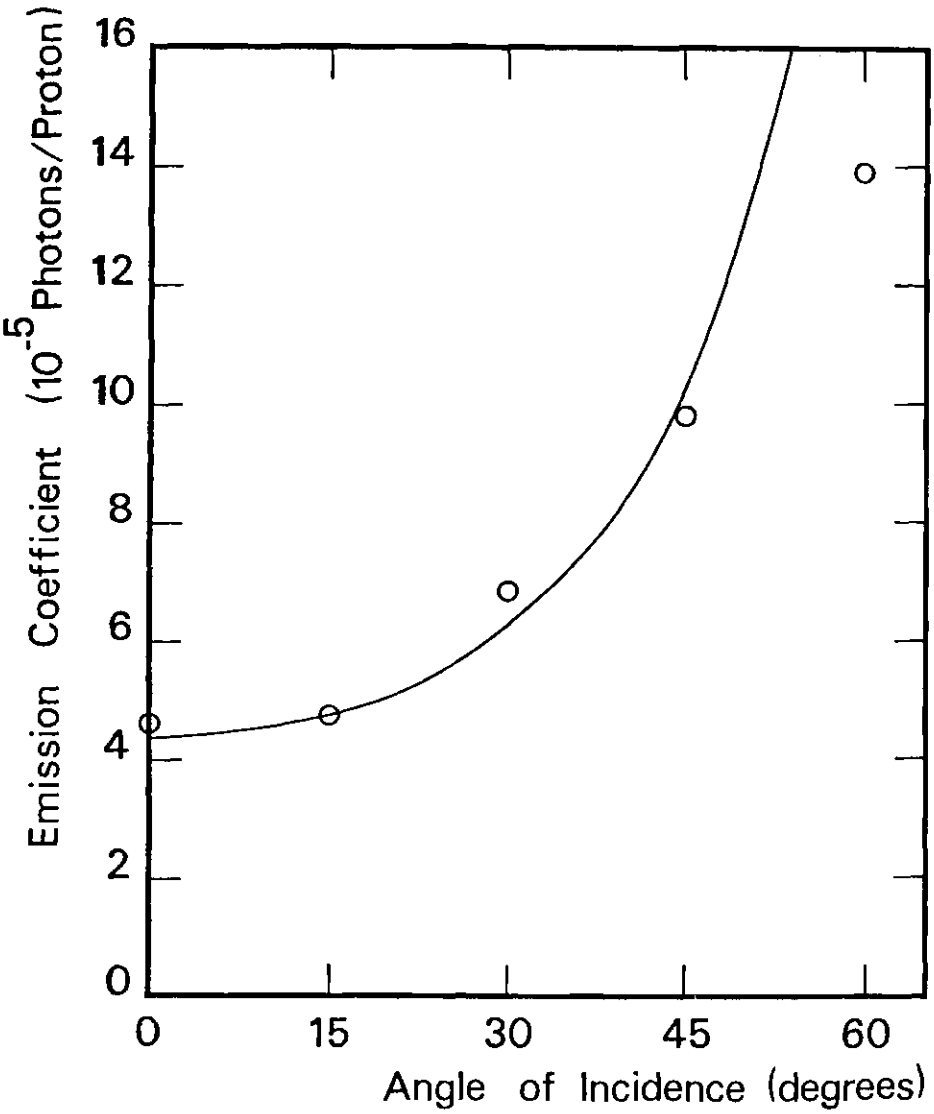

Figure 16. Emission Coefficient of the H (n = 3 to n = 2) Transition Shown as a Function of Angle of Incidence. (Experimental conditions: 25 KeV protons incident on Nb. Circles, experimental data points; solid line, predicted dependence with $A/a = 7.8 \times 10^7$ cm/sec. The predicted curve has been normalized to the data at 15^o incidence angle.)

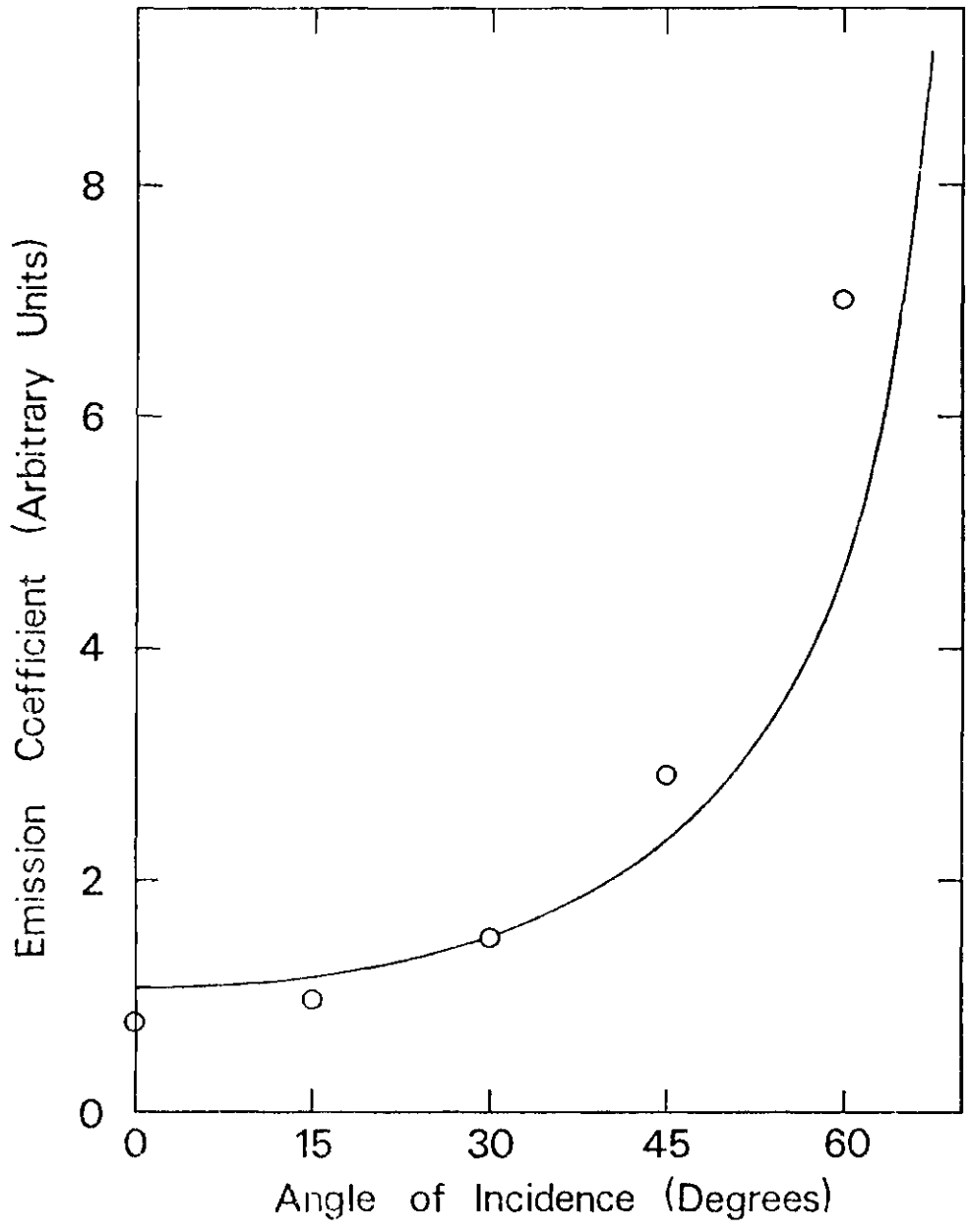

Figure 17. Emission Coefficient of the He $3^3D \rightarrow 2^3P$ Transition Shown as a Function of Angle of Incidence. (Experimental conditions: 30 KeV He^+ incident on Nb. Circles, experimental data points; solid line, predicted dependence with $A/a = 1.3 \times 10^8$ cm/sec. The predicted curve and the data (in arbitrary units) have been normalized together at 30° incidence angle.)

to be partially of a systematic nature. We have assumed in our model that the probability of excited-state formation is independent of incidence angle; the agreement observed in Figures 16 and 17 tends to support this assumption.

In order to illustrate the energy dependence of excitation and emission coefficients we present Figures 18 and 19. Figure 18 shows the case of He^+ ions incident on Cu at an incidence angle of 45^o; data points below 10 KeV are taken from relative values given by Kerkdijk and Thomas[1] which have been normalized to our data at 10 KeV. The predicted dependence of excitation coefficient on impact energy shows an average absolute percent deviation from our experimental values of emission coefficient of 9%. Figure 19 shows experimental emission coefficients for the cases of protons incident on Mo and on Cu at an incidence angle of 45^o; the predicted dependence of excitation coefficient on impact energy is shown for the case of protons on Mo and is normalized to the data at one point. Here the agreement between prediction and experiment is within the statistical variation of our data (± 6%) except at 10 KeV energy (30%). No explanation is given for this single discrepancy. For this prediction (as for the prediction in the case of He^+ on Cu) the value of A/a used is the "measured value reported in Chapter IV; for He^+ on Cu (He 3^3D state) this value is 3×10^8 cm /sec , and for H^+ on Mo (H n = 3 level) 7.8×10^7 cm /sec.

We have made some additional predictions for both these cases, by varying the value of A/a; all predictions for a given case have been normalized together at one point. In Figure 20, we show these predictions for

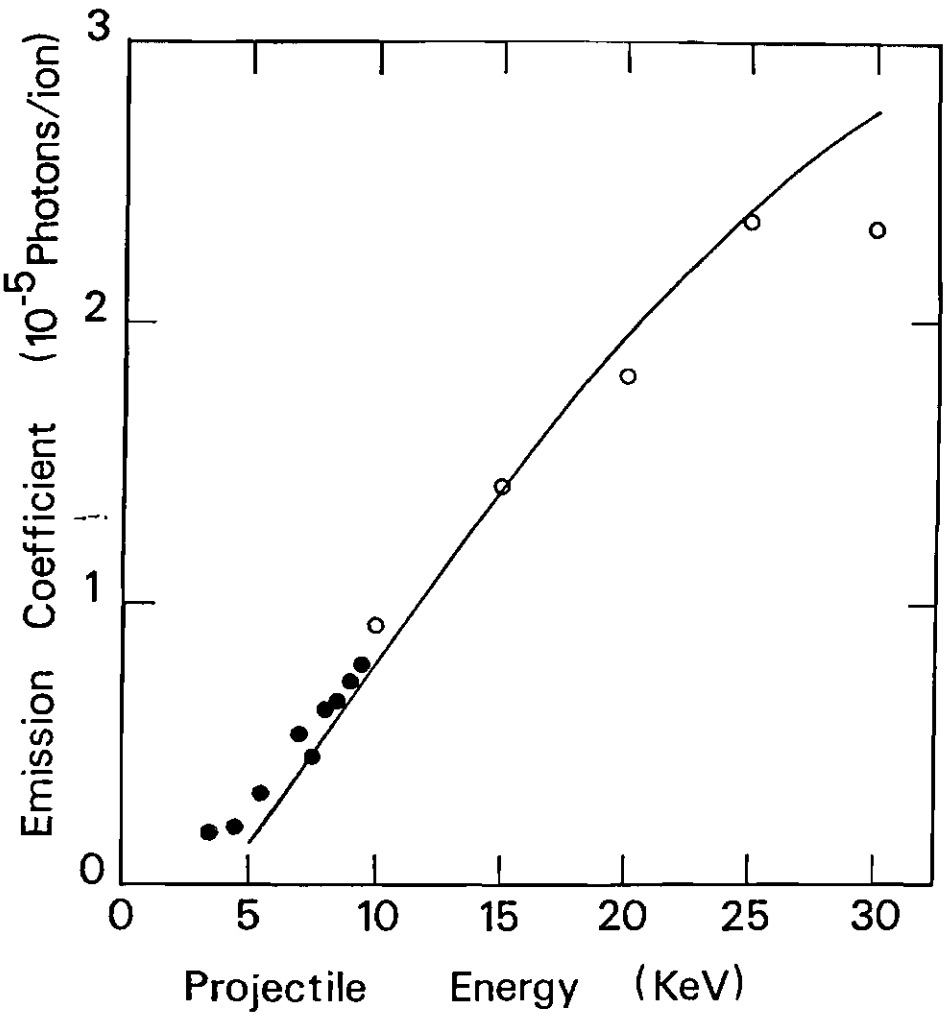

Figure 18. Emission Coefficient of the He $3^3D \rightarrow 2^3P$ Transition Shown as a Function of Projectile Energy. (Experimental conditions: He^+ incident on Cu at an angle of 45^o. Data points below 10 KeV are from Reference 1. The solid line is the prediction normalized to the experimental data at 15 KeV and calculated using a survival coefficient, A/a, of 3.0×10^8 cm/sec.)

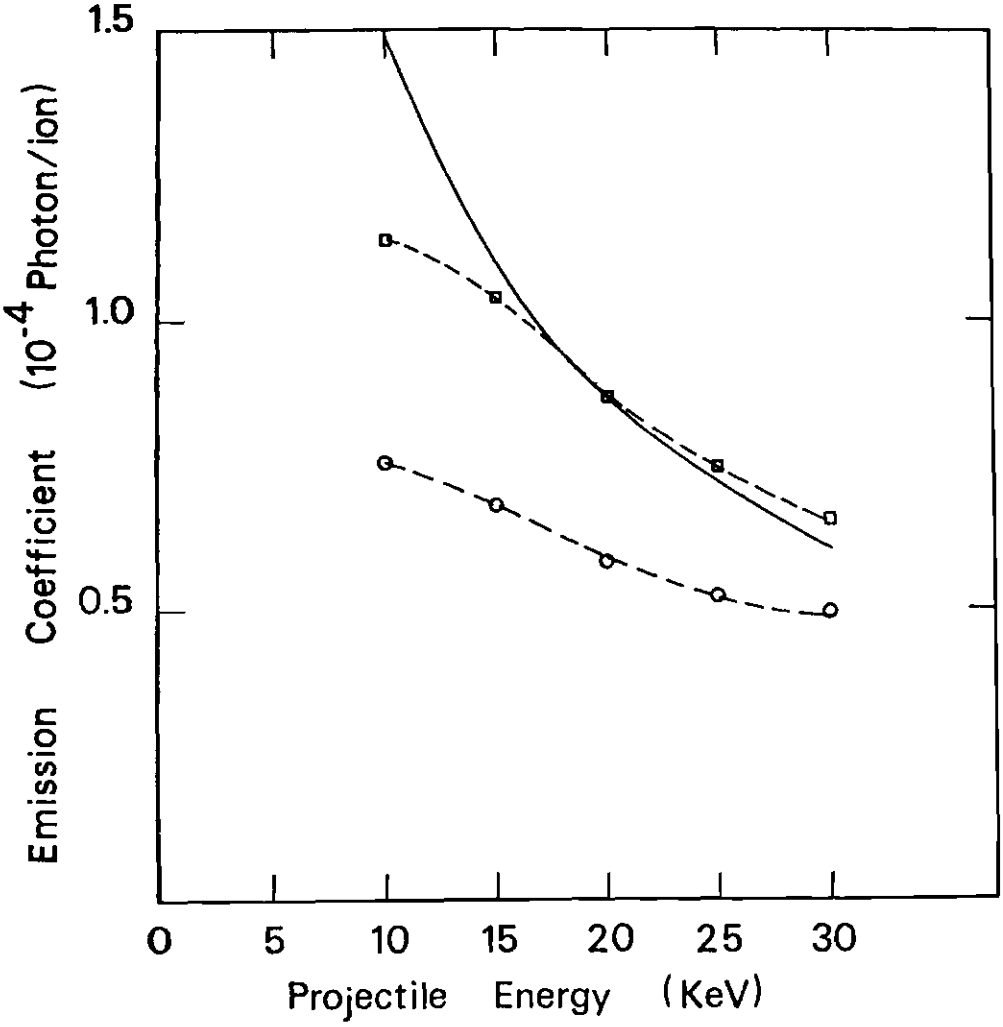

Figure 19. Emission Coefficient of the H (n = 3 to n = 2) Transition Shown as a Function of Projectile Energy. (Squares are data points for protons incident on Mo at an angle of 45°; circles are data points for protons incident on Cu at an angle of 45°; solid line is the predicted dependence for Mo with $A/a = 7.8 \times 10^7$ cm/sec. The predicted curve has been normalized to the Mo data at 20 KeV energy. Dashed lines indicate the general trend of the experimental data.)

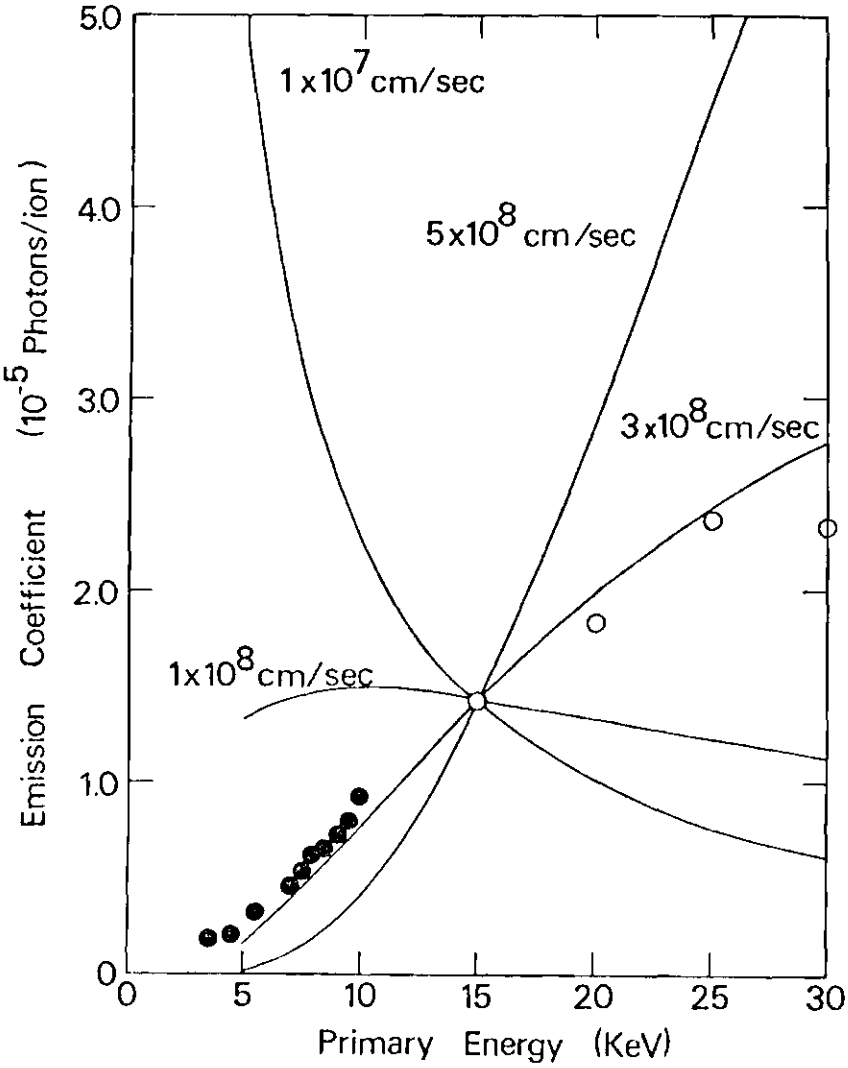

Figure 20. Predicted Emission Coefficient Energy Dependence of the He $3^3D \rightarrow 2^3P$ Transition Shown as a Function of Survival Coefficient. (Data points are for He^+ ions incident on Cu at an angle of 45°; data points below 10 KeV are from Reference 1. The solid lines are predictions using the indicated values of survival coefficient, A/a. The predictions are all normalized to the data at 15 KeV energy.

He^+ on Cu. Clearly the value 3×10^8 cm /sec "measured" by line shape analysis gives also the best agreement in the matter of energy dependence. In Figure 21, we show several predictions for the case of protons on Mo. The prediction we have made using a value of $A/a = 1 \times 10^8$ cm /sec lies within the statistical variation of the data (± 6%) except at 10 KeV energy (25%). Compared to our value of A/a "measured" by line shape analysis (7.8×10^7 cm /sec) this value is just outside the range of our 25% error estimate. Because the Balmer emission analyzed for these results includes three transitions from different upper states, with each state possibly exhibiting a different value of A/a, it is not surprising that the experimental data do not agree exactly with any of the predicted curves in Figure 21, nor with the curve predicted using the average "measured" value 7.8×10^7 cm /sec. Nevertheless, the agreement in both cases (He^+ on Cu and H^+ on Mo) of the experimental emission coefficients with the predicted energy dependence using the "measured" A/a values is such that we can draw the following conclusion: we based our model on the assumption that formation of a particular excited state is independent of impact energy; the good-to-fair results just mentioned support this assumption; thus we conclude that the excitation probability for a particular excited state is not a strong function of projectile energy in the range 5 to 30 KeV. This is consistent with a study by Berkner et al.[34] of the excited state fraction in hydrogen beams that had traversed thin metallic foils; they also concluded that the probability of excited-state formation varies very little with projectile energy. Furthermore, our additional predictions of energy dependence, using various values of A/a, reveal how sensitive the energy dependence is to the value of survival coefficient. Thus

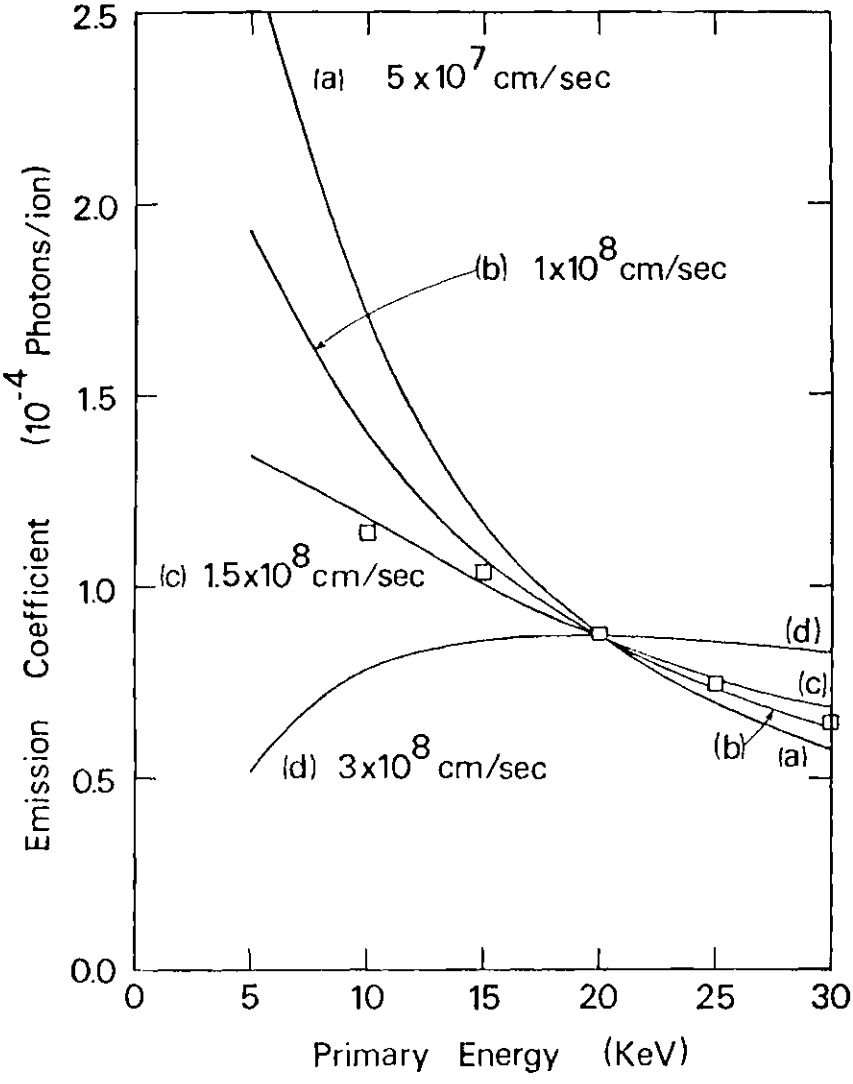

Figure 21. Predicted Emission Coefficient Energy Dependence of the H (n = 3 to n = 2) Transition Shown as a Function of Survival Coefficient. (Data points are for protons incident on Mo at an angle of 45°. The solid lines are predictions using the indicated values of survival coefficient, A/a. The predictions are all normalized to the data at 20 KeV energy.)

we have another indication of the dominant role of radiationless de-excitation processes in the interaction of backscattered H^+ and He^+ with metal surfaces. Because the energy dependence is such a sensitive function of A/a, it provides an alternative method of measuring A/a. Rather than varying A/a to provide a best fit to a line shape, the fitting may be done to the energy dependence of the emission coefficient. Such a procedure has already been used for the study of excited sputtered particles in the work of White and Tolk.[13]

Dependence of Coefficients on Target

A further result of our work is a measure of how the emission coefficient varies with target atomic number. The data are shown in Figures 22 and 23 for fixed impact energy and angle, for He^+ and H^+ projectiles, respectively. In general, the emission coefficient rises with atomic number although there is some irregularity in the behavior.

It is possible to make a theoretical estimate of this atomic-number dependence, again using the work of McCracken and Freeman.[2] The probability of backscattering with a given energy is related to the energy loss suffered by the projectile as it penetrates the target, as discussed in Chapter IV; loss is calculated using the Lindhard-Scharff[32] theory for electronic stopping. The backscattering probability is also related to a Rutherford-scattering event involving the projectile and target nuclei; this large-angle scattering event returns the projectile to the surface. The work of McCracken and Freeman[2] shows that the backscattering probability is proportional to a function f(Z), given in our Equation (21):

$$f(Z) = Z_1^{5/6} Z_2 \left(Z_1^{2/3} + Z_2^{2/3} \right)^{3/2} \qquad (32)$$

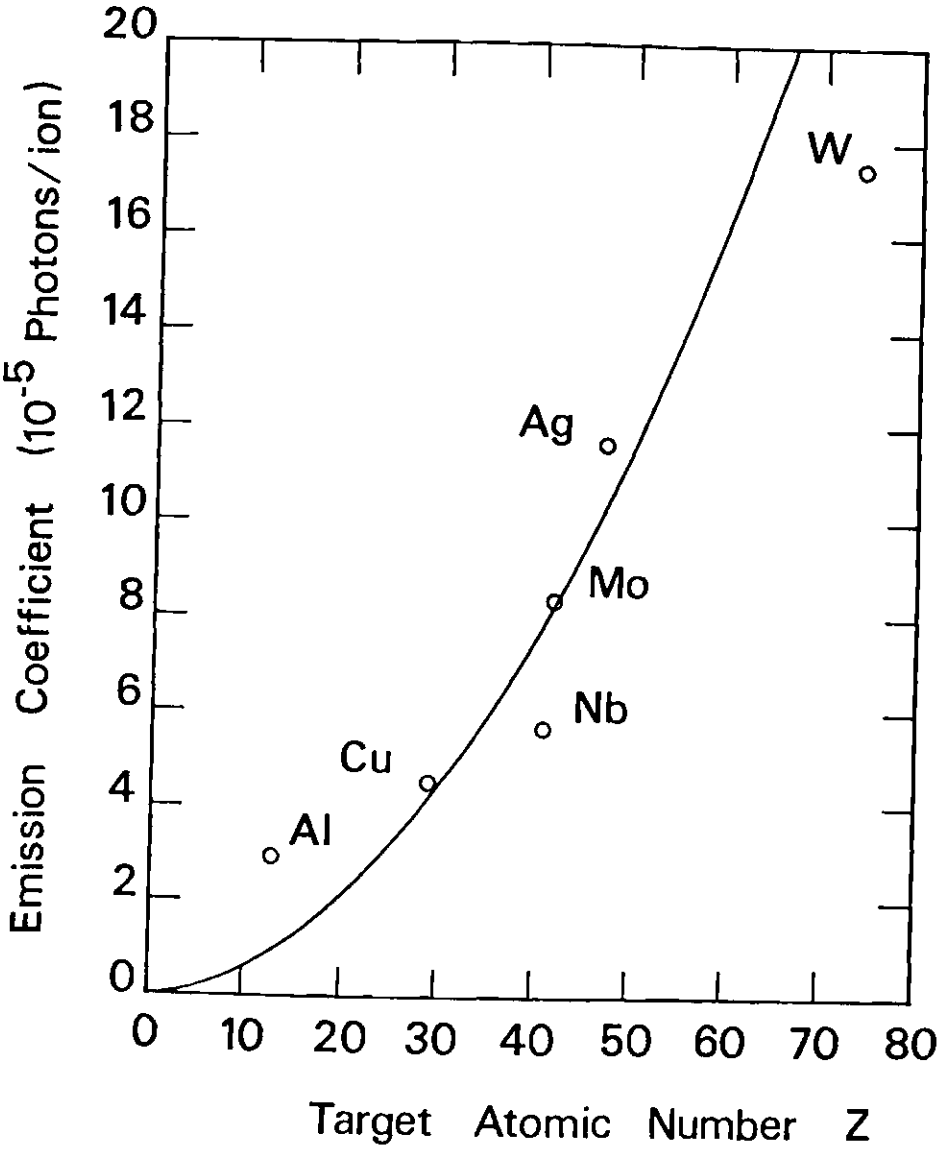

Figure 22. Emission Coefficient of the He $3^3D \rightarrow 2^3P$ Transition Shown as a Function of Target Atomic Number. (Experimental conditions: 25 KeV He^+ incident at an angle of 60^o. Circles, experimental data points; solid line, predicted dependence. The predicted curve has been normalized to the data at the Mo data point.)

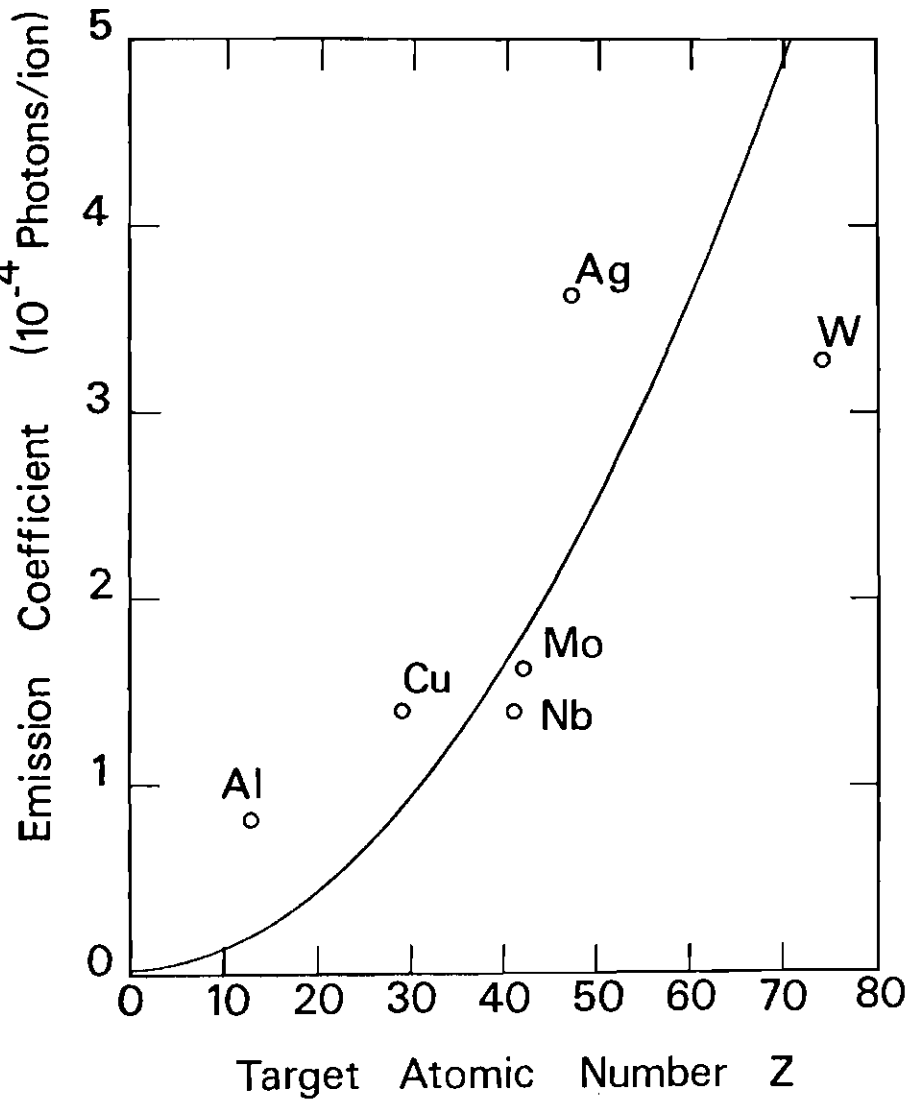

Figure 23. Emission Coefficient of the H (n = 3 to n = 2) Transition Shown as a Function of Target Atomic Number. (Experimental conditions: 25 KeV protons incident at an angle of 60°. Circles, experimental data points; solid line, predicted dependence. The predicted curve has been normalized to the data at a single point to provide a best fit.)

Here, Z_1 is the atomic number of the incident ion, and Z_2 is the atomic number of the target atom. In effect, the quantity dq of Equations (11) and (25) is proportional to the function f(Z). It follows then that a level-excitation coefficient should be proportional to f(Z); if we again make the assumption, presented in Chapter III, that excitation coefficients are proportional to emission coefficients, then the factor f(Z) will contain the functional dependence of emission coefficient on target atomic number. We have plotted f(Z) in Figures (22) and (23) normalized to the experimental data.

In the case of He (Figure 22) the average absolute percent deviation of the prediction from the data is 25%, and in the case of H (Figure 23), 40%. Thus, within these error limits, the backscattered excited-atom flux has the same dependence on target atomic number as is predicted for the total backscattered particle flux. It follows then that the excited-state fraction contained in the backscattered flux is not a sensitive function of the target itself; that is to say, the factor F of Equation (25) is not greatly dependent on the target atomic number. This is consistent with studies by Berkner et al.[34] of the excited-atom fraction in projectile beams that had traversed thin metallic foils; they also show that the fraction of excited atoms in the emergent projectile beam is not a sensitive function of the target.

CHAPTER VI

PROPOSED BOUND ELECTRON STATES IN THE WAKE OF SWIFT PROTONS IN ALUMINUM AND COPPER

Our final investigation consisted of a search for radiative evidences of a phenomenon predicted theoretically by Neelavathi, Ritchie, and Brandt.[6] According to them, a fast charged particle moving through a solid is followed by a cylindrically symmetric wake of electron-density fluctuations, where the particle track defines the axis of the wake. This wake consists of a series of domains, at distinct distances behind the projectile, in which the electron density is alternately enhanced and depleted relative to the mean density in the medium. Domains of density enhancement create regions of negative electric potential, and domains of depletion create regions of positive potential. If sufficiently deep, these potential troughs can trap, respectively, positive or negative particles and sweep them along in wake-riding states trailing the projectile. In the case of a positively charged projectile traversing a metal, metal electrons would be trapped at definite distances behind the projectile with binding energies ranging from ~ 10 eV behind protons to several hundred eV behind highly charged heavy ions. As the positively charged particle left the metal, the electron-density troughs would disappear. Thus the energy released by the previously trapped electrons would be emitted radiatively, and could be detected by observing the point of exit from the metal of the projectile. For incident protons the projectile

energy required is of the order of one MeV. For a proton of one MeV energy, the binding energy of an electron in the first trough of the oscillating potential created in a medium like aluminum is ~ 7.5 eV; this is at a distance behind the proton of 44 Å. The three successive troughs occur at distances of 103 Å, 161 Å, and 220 Å; the approximate binding energies of an electron for these three troughs are, respectively, 5.7 eV, 4.3 eV, and 3.2 eV. Succeeding troughs in the electron-density fluctuation will be at greater distances and will present still smaller binding energies.

Thus our task was to use an optical detection system to examine the radiation present (if any) at the point of exit for protons having traversed a thin piece of aluminum. We chose aluminum foil of thickness ~ 1 μ to reduce the energy loss of the protons to ~ 5%.[35] For primary proton energies we used 650 keV and 900 keV. Our results were that we observed no optical emissions which could arise from the above phenomenon. A broad band in the region 3000-4000 Å was found to be the result of fluorescence (under reflected ion impact) of the quartz window used for observation. We also examined the point of entrance for protons incident on aluminum; again we found no evidence of the proposed phenomenon. In addition we repeated the experiment using copper foil of thickness ~ 1 μ; our results were negative in this case as well.

Recently, at the conference on Atomic Collisions in Solids (Amsterdam, The Netherlands, September 1975), Professor W. Brandt of New York University stated that the calculations of Neelavathi and Ritchie are incorrect and there should be no oscillations behind protons that are capable of trapping electrons. Also Day[36] has come to a similar conclusion.

Thus our negative results for this test would seem to be in accord with the most recent theoretical treatment of the subject.

CHAPTER VII

CONCLUSIONS

From our analysis of line shape (Chapter IV) we conclude that excited atoms recoiling from a target have a high probability of radiationless transition. For example, using a measured value of A/a (1.0×10^8 cm /sec) in Equation (4) to calculate the probability $p(V_\perp)$ that a 30 KeV ($V = 1.2 \times 10^8$ cm /sec) 3^3D helium atom recoiling normal to a molybdenum surface will not undergo radiationless transition, we get $p(V_\perp) = \exp(- 1.0/1.2) = 0.43$. Thus only 43% of these rather fast recoils escape without radiationless transition. For slower recoils, which are in the majority, the survival probability is correspondingly less. We summarize in Table 5 the values of survival coefficient, A/a, which we have determined by line shape analysis.

We are now in a position to understand why the "surface-scattering" model of Kerkdijk and Thomas[1] gave a roughly accurate prediction of line shape. That earlier work assumed, arbitrarily, that only fast atoms scattered elastically from the surface emerge in an excited state. We have shown here that particles scattered at all depths in the solid may in fact emerge in an excited state, but only those of highest velocity have any substantial probability of surviving radiationless transition; these faster atoms arise from scattering close to the surface. Thus the principal contribution to line shape does in fact arise from the scattered flux component considered by Kerkdijk and Thomas.[1]

Table 5. Values of Survival Coefficient A/a Obtained by Line Shape Analysis

Projectile	Atomic State Formed	Survival Coefficient A/a (cm/sec) by Target Metal		
		Niobium	Copper	Molybdenum
	He 3^3D	1.3×10^8	3.0×10^8	1.0×10^8
He^+	He 4^3D	0.8×10^8	1.6×10^8	
	He 3^3P	1.5×10^8		
H^+	H n = 3		7.8×10^7 *	

*average for the three metals

Experimentally, we are unable to determine which of the two previously mentioned radiationless processes (resonance ionization and Auger de-excitation) is dominant for our conditions. With this understanding, our review of the values of A/a given by other researchers presents no contradiction to our results. For Auger de-excitation of $He(2^3S)$ at an Mo surface, Cobas and Lamb[20] predict $A/a = 1.3 \times 10^8$ cm /sec which is quite comparable with our measured values. Experimentally, Smits[23] and Kerkdijk[24] determine a value of $A/a = 1.5 \times 10^8$ cm /sec for the n = 4 state of H; this also is quite comparable with our measured values.

With our values of A/a measured by line shape analysis, we are further able to predict by our simple model the functional dependence of the level-excitation coefficients on such parameters as projectile impact energy and projectile impact angle (Chapter V). The model also permits a prediction of excitation coefficient as a function of target atomic number. Agreement between experimental evidence and our predictions is very satisfactory in view of the simplicity of the model utilized. We have throughout assumed that the probability of a backscattered atom emerging at the surface in an excited state is independent of its direction, speed, and the nature of the target. This assumption seems to be reasonably valid, and certainly the excited-state population is a very weak function of these parameters. We have also shown that the dependence of emission coefficient on primary projectile energy is a quite sensitive function of survival coefficient. Our work provides measured absolute values of the emission coefficients and some estimates of the absolute values of the level-excitation coefficients. On the basis of our measured values of emission coefficients and our determinations of survival coefficient, we

estimate that less than 1% of all incident projectiles recoil as excited atoms.

The major gap in our understanding of the whole problem (and in that of earlier work[1,5,13]) is the lack of information on the process by which the excited atom is created; for this reason we are unable to assign absolute values to our predictions of excitation coefficients. Yavlinskii et al.[37] suggests that a proton is neutralized as it finally emerges from the target; the neutralization is supposed to take place by a process of three-body recombination in the surface layer of electrons. We would note that, on theoretical grounds, recombination in a plasma should be primarily to d states[38]; moreover, the afterglows of high-density helium plasmas show[39] atomic lines that are principally from 3^3D, 4^3D, and 3^3P states. Thus the spectra observed in our work are qualitatively similar to those observed in the decaying-plasma situation, where a three-body recombination process is expected to be a primary source of excited atoms. Application of the results of Yavlinskii et al.[37] to our line shape model made negligible difference in the predicted form of the spectral line.

Finally, we conclude in the matter of bound electron states in the wake of swift protons in aluminum and copper that the proposed emitted radiation is either non-existent or too weak to be detected by our present experimental arrangement. This is in agreement with the recent theoretical work of Day.[36]

APPENDIX

POLISHING PROCEDURE

All targets were first mechanically polished with 1 μ alumina grit (Al_2O_3). Then those which could not be electropolished (Nb, Ag, and W) were further mechanically polished with 0.3 μ alumina grit; in each case the lubricant used was distilled water. These finally were rinsed with methanol and dried with nitrogen gas.

In order to electropolish the metals Al, Cu, and Mo, an electrolytic solution was prepared from 250 ml. C_2H_5OH (absolute ethanol), 140 ml. H_3PO_4 (85% phosphoric acid), and 10 ml. H_2O (distilled water). This mixture was placed in a beaker whose inner surface was lined with a thin piece of stainless steel (the cathode). The metal sample (the anode) was then placed just below the level of the solution and a potential difference applied between the two electrodes. The magnitude of this voltage for a particular metal could be roughly inferred from the literature and was ultimately determined by trial and error. The objective was to polish the metal sample rather than etch, producing a surface which was smooth as well as clean. For the case of Cu an additional two grams of CuO (copper oxide) was dissolved in the electrolytic mixture. When the electropolishing was complete, the samples were removed, rinsed with methanol, and dried with nitrogen gas. Storage of samples for one or two days was accomplished in an airtight dessicator.

REFERENCES

1. C. Kerkdijk and E. W. Thomas, Physica 63, 577 (1973).

2. G. M. McCracken and N. J. Freeman, J. Phys. B 2, 661 (1969).

3. H. D. Hagstrum, Phys. Rev. 96, 336 (1954).

4. L. J. Varnerin, Jr., Phys. Rev. 91, 859 (1953).

5. W. F. Van der Weg and D. J. Bierman, Physica 44, 206 (1969).

6. V. N. Neelavathi, R. H. Ritchie, and W. Brandt, Phys. Rev. Lett. 33, 302 (1974).

7. R. M. Chaudhri, M. Y. Khan, and A. L. Taseer, Nature 177, 1226 (1956).

8. A. A. Sterk, C. L. Marks, and W. P. Saylor, Phys. Rev. Lett. 17, 1037 (1966).

9. V. V. Gritsyna, T. S. Kijan, A. G. Koval', and Ja. M. Fogel', Phys. Lett. 27A, 292 (1968).

10. V. V. Gritsyna, T. S. Kijan, A. G. Koval', and Ja. M. Fogel', ZhETF Pis. Red. 9, 212 (1969).

11. V. V. Gritsyna, T. S. Kijan, A. G. Koval', and Ja. M. Fogel', Zh. Eksp. Teor. Fiz. 58, 1491 (1970).

12. G. M. McCracken and S. K. Erents, Phys. Lett. 31A, 429 (1970).

13. C. W. White and N. H. Tolk, Phys. Rev. Lett. 26, 486 (1971).

14. N. H. Tolk, D. L. Simms, E. B. Foley, and C. W. White, Radiation Effects 18, 221 (1973).

15. M. Zivitz and E. W. Thomas, to be published in Phys. Rev. B.

16. P. Meischner and H. Verbeek, J. Nucl. Material 53, 276 (1974).

17. O. B. Firsov, E. S. Mashkova, and V. A. Molchanov, Radiation Effects 18, 257 (1973).

18. R. L. Erickson and D. P. Smith, Phys. Rev. Lett. 34, 297 (1975).

REFERENCES (Continued)

19. S. S. Shekhter, Zh. Eksp. Teor. Fiz. 7, 750 (1937).

20. A. Cobas and W. E. Lamb, Phys. Rev. 65, 327 (1944).

21. J. I. Gersten and N. Tzoar, Phys. Rev. B 9, 4038 (1974).

22. R. K. Janev, I. V. Terzic, and D. M. Davidovic, Surface Science 26, 142 (1971).

23. S. Smits, Doctoral Dissertation, FOM-Institut voor Atoom--en Molecuulfysica, Amsterdam, The Netherlands (1974).

24. C. Kerkdijk, Doctoral Dissertation, University of Leiden, The Netherlands (1975).

25. R. Stair, R. G. Johnston, and E. W. Halbach, J. Res. Natl. Bur. Stand. (U.S.) 64A, 291 (1960).

26. J. W. McConkey, J. Opt. Soc. Am. 59, 110 (1969).

27. J. F. M. Aarts and F. J. de Heer, J. Opt. Soc. Am. 58, 1666 (1968).

28. E. W. Thomas, G. D. Bent, and J. L. Edwards, Phys. Rev. 165, 32 (1968).

29. D. J. Burns, F. R. Simpson, and J. W. McConkey, J. Phys. B 2, 52 (1969).

30. W. L. Wiese, M. W. Smith, and B. M. Miles, Atomic Transition Probabilities, National Bureau of Standards (U.S. GPO, Washington, D.C., 1969).

31. E. W. Thomas, Excitation in Heavy Particle Collisions (Wiley-Interscience, New York, 1972), p. 13.

32. J. Lindhard and M. Scharff, Phys. Rev. 124, 128 (1961).

33. E. Everhart, G. Stone, and R. J. Carbone, Phys. Rev. 99, 1287 (1955).

34. K. H. Berkner, I. Bornstein, R. V. Pyle, and J. W. Stearns, Phys. Rev. A 6, 278 (1972).

35. S. Flügge, Encyclopedia of Physics (Springer-Verlag, Berlin--Göttingen--Heidelberg, 1958), Vol. XXXIV, p. 193.

36. M. H. Day, Phys. Rev. B 12, 514 (1975).

REFERENCES (Concluded)

37. Yu. N. Yavlinskii, B. A. Trubnikov, and V. F. Elesin, Bull. Acad. Sci. USSR Phys. Ser. 30, 2135 (1966).

38. N. D'Angelo, Phys. Rev. 121, 505 (1961).

39. Dr. Cunningham, University of Texas (private communication).

VITA

William E. Baird, Jr. was born in Macon, Georgia, on February 8, 1949. He is the son of William Eugene Baird and Addie Marie McKellar Baird.

Mr. Baird is a graduate of Lanier High School, Macon, Georgia (1965) and of Emory University, Atlanta, Georgia (1969). During the years 1969-1971 he was on the faculty at St. Andrew's School, Middletown, Delaware. He received the degree Master of Science in Physics from the Georgia Institute of Technology (1972). During his graduate program he held graduate teaching and research assistantships. He is presently on the faculty at Oxford College of Emory University, Oxford, Georgia.

Mr. Baird is a member of Phi Beta Kappa, the American Association of Physics Teachers, and Sigma Pi Sigma.